Continuous-Operation Modular Rotating Fusion Engine

Iván Moreno Gil

September 18, 2025

Abstract

This invention describes a ***Continuous-Operation Rotating Modular Fusion Engine–Reactor*** based on a **rotating and modular architecture**, composed of a plurality of independent **polyhedral fusion cells** (preferably **hexagonal pyramids**) arranged radially around a central rotor. Each cell integrates deuterium–tritium fuel pellet injection systems, ignition modules (lasers or equivalent drivers), and diagnostic/control ports located at the structural vertices. The flat base of each cell functions as a *hot plate*, coupled to a shared **neutron energy harvesting and conversion blanket** (Neutron Energy Harvester, NEH) manufactured with advanced materials (W–SiC, RAFM), and further supported by an integrated **IGBI radiator plate** that enhances lateral heat spreading, improves Brayton efficiency, and reduces thermomechanical stress.

The rotation of the rotor imposes a cyclic sequence: *injection* → *ignition* → *energy release* → *cooling*, distributed in parallel across the **dozens of cells per rotor** and, at plant scale, across **thousands of cells coordinated in multi-rotor campuses**. This configuration **ensures continuous electricity production**, in contrast to the discrete discharges of inertial confinement, and offers a **modular and scalable pathway** compared to the monolithic chambers of tokamaks. The design incorporates staged thermal management, replaceable hot-plate cartridges, the integrated IGBI radiator, and optional magnetohydrodynamic (MHD) conversion, ensuring high efficiency, simplified maintenance, and fault tolerance.

Technical Field The invention belongs to the field of **nuclear fusion reactors**, with specific application to **modular rotating architectures for continuous operation**. Its primary objective is the **steady generation of electrical power** with high power density and rapid industrial scalability, although the same technology can also be extended to **long-range space propulsion systems**.

Contents

1 Background of the Invention

Conventional fusion systems include:

- **Tokamaks and stellarators:** large toroidal chambers based on continuous magnetic confinement, requiring intense fields ($B \sim 5$–10 T), complex cryogenic systems, and structures on the order of tens of meters. Although they have demonstrated sustained plasma confinement for several seconds, they suffer from MHD instabilities, disruptions, and high maintenance costs. See "ITER Physics Basis" [1], Pedersen et al. [2], and Federici et al. [3].
- **Inertial confinement fusion (ICF):** spherical targets compressed by high-energy lasers in nanosecond pulses, as in the NIF or OMEGA facilities. They have achieved *scientific gain* ($Q_{\text{fus}} > 1$) in single-shot demonstrations, but repetition at high cadence (> 1 Hz) remains unsolved in practice due to optical damage, pellet logistics, and driver energy costs. See Le Pape et al. [4], Hurricane et al. [5], and Meyerhofer et al. [6].
- **Multi-chamber or sequential ignition proposals:** such as Dubrovsky (2023) and Woodruff (2010), which proposed distributing ignition across multiple targets or secondary chambers. While conceptually mitigating localized loads, they have not proposed industrializable architectures nor solutions for continuous heat and neutron management, see Dubrovsky [7] and Woodruff [8].

These approaches face recurring limitations:

1. **Concentrated neutron loading:** highly localized fluxes rapidly degrade first walls ($\sim$MW/m^2), requiring frequent replacements, see Federici et al. [3] and Zinkle and Ghoniem [9].
2. **Restricted duty cycles:** both superconducting magnets and laser systems suffer from thermal and radiation fatigue, reducing availability to scales of days or weeks. See Devred et al. [10] and Zinkle and Ghoniem [9].
3. **Lack of continuous operation:** none of the current systems achieve a stable baseload regime comparable to fission or combined cycles. See Stacey [11] and Agency [12].

There is therefore a need for an architecture that:

- Distributes neutron and thermal loads spatially and temporally.
- Simplifies driver requirements by distributing ignition across multiple smaller chambers.
- Enables industrial modularity: progressive scaling from tens of MW to GW without fundamental redesign.
- Provides intrinsic fault tolerance, eliminating the risk of catastrophic interruption from a single-cell failure.
- Operates in continuous mode, making its commercial use viable as a clean energy producer.

1.1 Motivation and Safety Justification

The main motivation of this invention lies in the broad safety margin offered by modular fusion architectures compared to fission reactors and monolithic confinement systems. See Dean [13] and Maisonnier et al. [14]. Key differences include:

- **Absence of sustained chain reaction.** Each cell requires an external driver pulse and a fuel pellet; without them, fusion ceases instantly. No runaway conditions exist.
- **Minimal fuel inventory.** Active fuel is limited to milligrams of D–T per ignition. Even at full-plant scale, the circulating quantity corresponds only to grams, compared to tons of fissile uranium or plutonium in conventional reactors. See International Atomic Energy Agency [15].
- **No residual decay heat.** In a shutdown (driver SCRAM or seismic trigger), all thermal generation halts within microseconds. Unlike fission, there is no residual power that threatens overheating, see Zohuri [16].
- **Seismic and impact resilience.** In the event of earthquakes or external impacts, the maximum consequence is shielding damage and possible release of small traces of tritium or activated structural material. There is no possibility of a Chernobyl- or Fukushima-type accident. For more information, see Cadwallader [17] and Federici et al. [18].
- **Engineered confinement.** The reactor is housed in reinforced concrete vaults with 1.5–2 m biological shields. Robotic handling and modular cartridges minimize exposure during maintenance.

This safety profile enables siting plants closer to consumption centers, reduces emergency planning zones, and differentiates the Modular Rotating Fusion Engine (MRFE) substantially from fission plants and monolithic fusion facilities.

2 Summary of the Invention

The invention proposes a **Modular Rotating Fusion Engine (MRFE)** whose novelty resides in the *geometry and mechanics* of the system rather than in speculative or undeveloped technologies. The concept is structured around:

1. A rotor integrating multiple **polyhedral fusion cells** (we use as example **hexagonal pyramids**) arranged radially, each acting as a repetitive micro-fusion chamber.
2. Each cell undergoes an autonomous cycle: *pellet injection* → *laser ignition* → *energy absorption in the NEH blanket* → *staged cooling*, with characteristic cooling times $\tau_{\mathrm{cool}} \sim 5$ s, enabling continuous reuse.
3. A **shared Neutron Energy Harvester (NEH) blanket** within each cell, composed of functional layers (plasma-facing, moderator, breeder/coolant, structural shielding) to absorb neutron flux, breed tritium, and extract usable heat.
4. **Dual energy conversion:** (i) via Brayton/sCO_2 thermodynamic cycles for recovered heat, and (ii) optionally via **MHD channels** at cell edges, directly converting a fraction of charged-particle energy into electricity.
5. A rotating configuration in which hot faces sequentially couple to fixed radiator/heat-exchanger stations, thereby avoiding thermal shocks and distributing loads evenly. Thermal coupling is realized through an integrated **IGBI radiator plate** (Impinging Gas Bearing Interface), combining helium microjets with high-conductivity pin–fin surfaces for efficient lateral heat spreading.
6. Modular scalability: from 24 up to 120 cells per rotor or more; rotors can be stacked axially or operated in parallel to assemble multi-GW plants. Progressive commissioning allows electricity generation to begin with the very first rotor.
7. Fault tolerance: a defective or failed cell reduces total output by less than 2% in a 60-cell rotor, maintaining continuous operation without systemic risk.

In summary, the MRFE provides an alternative to traditional fusion approaches by leveraging **existing industrially mature technologies**: high-energy Nd:glass lasers, see Campbell and Glenzer [19] and al. [20]; first-wall materials such as RAFM steels and W–SiC composites, see Zinkle and Busby [21] and al. [22]; Brayton/sCO_2 thermodynamic cycles, see al. [23]; advanced metallic additive manufacturing (WAAM, SPF/DB), see Martina et al. [24] and al. [25]; and robotized remote-handling systems, see Taylor and Davis [26]. ***The true innovation lies in the rotating modular architecture and the integrated IGBI radiator plate, not in the development of the base technologies.***

3 Claims

1. **(Rotating architecture and continuous regime)** A rotating fusion reactor comprising a rotor with multiple independent polyhedral fusion cells, configured to receive fuel and ignition pulses, wherein the cells sequentially rotate through injection, ignition, energy extraction, and cooling, maintaining a continuous energy production regime.

2. **(Preferred cell geometry)** The reactor of claim 1, wherein the cells are **hexagonal pyramids** with their bases acting as *hot faces* aligned with fixed radiator/heat exchanger stations.

3. **(Alternative geometries)** The reactor of claim 1, wherein the cells are alternatively pentagonal pyramids, triangular pyramids, or other convex polyhedra providing flat hot faces compatible with stationary thermal coupling.

4. **(Multilayer NEH blanket)** The reactor of any of the preceding claims, comprising a *Neutron Energy Harvester (NEH)* multilayer blanket including: (i) a plasma-facing component in W or W–SiC, (ii) an intermediate moderator, (iii) breeder/coolant channels with LiPb or FLiBe, and (iv) a structural shield in reduced-activation ferritic–martensitic (RAFM) steels or functional equivalents.

5. **(NEH dome coupled to hot face)** The reactor of any of the preceding claims, comprising an *NEH dome* coupled to the hot face of each cell, configured as a prism or truncated pyramid *congruent* with the cell geometry, integrating functional layers, sniper-holes, coolant manifolds, and mechanical/electrical couplings in a **replaceable cartridge**, see Fig. 5.

6. **(Ignition drivers)** The reactor of any of the preceding claims, wherein ignition drivers (lasers, ion beams, or equivalents) are mounted at the apex and/or edges of the cells, delivering synchronized pulses with a delay of less than 10 ps.

7. **(Cell-per-rotor scale)** The reactor of claim 1, wherein the rotor couples to a central *bus* and accommodates between **24 and 120 cells or more per rotor**, with possible concentric rings and/or axial stacking, enabled by the intrinsic modularity of the architecture.

8. **(Interchangeable modular cartridge)** The reactor of any of the preceding claims, comprising a **modular interchangeable cartridge** on the hot face of each cell, removable and insertable by robotic means during continuous operation.

9. **(Frictionless thermal interface)** The reactor of any of the preceding claims, comprising a **thermal interface system** between the hot face and the stationary radiator, based on capillary liquid films, isothermal coupling, or pressurized helium jet systems (**IGBI radiator interface**), or other frictionless interfaces designed to transfer heat with minimal wear.

10. **(Direct conversion)** The reactor of any of the preceding claims, wherein *optionally* metallic liquid coolant channels (LiPb, doped FLiBe, or conductive equivalents) are installed to act as **magnetohydrodynamic (MHD) ducts** for direct electrical energy conversion (see Appendix A).

11. **(Rotor thermal-gradient mitigation)** The reactor of any of the preceding claims, further comprising a **rotor thermal-gradient mitigation system** configured to maintain the temperature of the bearing ring within a predetermined margin and reduce differential expansion relative to the cells; wherein the preferred embodiment is an *isothermal IGBI radiator ring* with internal cooling channels, and *alternatively* flexible cooled interfaces or equivalent variants may be used to achieve the same function.

12. **(Cell-level fault tolerance)** The reactor of any of the preceding claims, wherein the functional independence of each cell provides fault tolerance, such that isolated ignition failures or off-nominal events cause only proportional power reductions without compromising overall rotor operation.

13. **(Optics and sensor protection)** The reactor of any of the preceding claims, wherein optics and sensors are protected by replaceable shields and barriers, including sacrificial windows and ceramic shutters, robotically interchangeable.

14. **(Low-activation structural materials)** The reactor of any of the preceding claims, wherein back plates and support structures are fabricated in **RAFM steel** or other low-activation equivalents, improving thermal conductivity, radiation resistance, and cost.

15. **(Additive manufacturing and lightweighting)** The reactor of any of the preceding claims, wherein cells and modular cartridges are manufactured by **metal additive manufacturing technologies** (WAAM, L-PBF, SPF/DB), incorporating *topological lightweighting* and *lattices* of equivalent stiffness to reduce mass and unit cost.

16. **(Staged cooling)** The reactor of any of the preceding claims, further comprising a **staged cooling system**, wherein hot faces are sequentially coupled with fixed radiators at the external station, distributing the thermal load of the cycle evenly.

17. **(Plant scalability)** The reactor of any of the preceding claims, wherein the modularity of cells and rotors allows configurations ranging from a **single rotor** (tens of MW) to **multi-rotor campuses** (hundreds of MW up to several GW), with progressive commissioning from the first installed rotor.

Correspondence with detailed description. Each of the above claims is supported by the technical sections of the document:

- Claim 1 → Sections 4.1 and 4.3
- Claim 2 → Section 4.1
- Claim 3 → Section 4.1
- Claim 4 → Sections 4.4 and 4.8 (multilayer NEH blanket)
- Claim 5 → Section 4.5 (detailed NEH dome architecture)
- Claim 6 → Section 5.4 (ignition drivers and synchronization)
- Claim 7 → Section 4.2 (scaling to 120 cells per rotor)
- Claim 8 → Section 5.5 (interchangeable modular cartridges)
- Claim 9 → Sections 5.1 and 4.6 (capillary/frictionless thermal interface, IGBI)
- Claim 10 → Section 5.3 (MHD liquid-metal coolant channels)
- Claim 11 → Section 4.2 (isothermal IGBI ring and thermal management)
- Claim 12 → Section 4.4 (fault tolerance of independent cells)
- Claim 13 → Section 5.4 (optics and sensors protected by barriers)

4 Detailed Description of the Invention

The following description presents a preferred embodiment of the rotating fusion reactor. The architecture is intrinsically **modular and adaptable**: the polyhedral cells may adopt different geometries (e.g., hexagonal pyramids, pentagonal pyramids, or tetrahedra), the number of cells per rotor is configurable, and the shaft length defines the number of stacked *floors* or *layers*. The example below is *illustrative and non-limiting*.

4.1 Hexagonal Pyramid Fusion Cell (Individual Module)

Each cell is the minimum modular unit of the MRFE. In this reference configuration a **regular hexagonal pyramid** with side $s \approx 1.0$ m (compact option $s = 0.5$ m) and height $h \approx 0.816\,s$ is used. The cell integrates structural containment, fusion energy capture, neutron protection, and primary thermal conversion.

Structural envelope.

- **Geometry:** regular hexagonal pyramid, base side $s \approx 1$ m, height $h \approx 0.82$ m.
- **Base material: RAFM steel** (reduced activation) in casing and edges, with lattice-type stiffeners (WAAM/HIP).
- **Thickness:** 18–25 mm in lateral faces; reinforced to 25–35 mm in anchoring sockets.
- **Function:** structural support, mechanical interface with the rotor, routing of sensors and manifolds, and secondary heat conduction to peripheral cooling.
- *Option* (Appendix A): Ti–6Al–4V (grade 5) in reduced-mass versions or in specific regions of low delayed activation.

Hot-plate.

- **Position:** flat hexagonal base of the pyramid, facing the ignition focal zone.
- **Materials: W–SiC tiles** (15–25 mm) over a **RAFM backplate** (25–30 mm).
- **Function:** α-particle stopping, first spectral conditioning of neutrons, heat extraction toward the NEH dome and circuits.
- **Thermal interface at station (IGBI):** dissipation to a stationary radiator via pressurized helium *impinging jets* combined with high-conductivity metallic *pin–fins* (heat removal capacity > 10 MW per station), with helium recirculation to a recuperator coupled to a Brayton/sCO_2 cycle.

Multilayer NEH dome (integrated in cartridge).

- **Geometry:** truncated hexagonal prism/dome coupled to the hot-plate, vertex-to-vertex, encapsulating the ignition focus. Interior radius to focus configurable (30–60 mm).
- **Reference stack:**
  1. **PFC** W–SiC: 20–30 mm.
  2. **Breeder/coolant FLiBe** in microchannels (active layer 60–80 mm).
  3. **Thermal absorber B_4C**: 5–10 mm.
  4. **Backplate RAFM**: 20–30 mm with *manifolds*.
- **Function:** high neutron capture fraction ($\varepsilon_{\text{cap}} \sim 0.8$–$0.9$), tritium breeding (^{6}Li in FLiBe), and main route of thermal extraction.
- *Option* (Appendix A): eutectic LiPb (17Li–83Pb) for variants with direct MHD conversion.

Service ports and drivers.

- **Pellet injection:** cryogenic line with injector and alignment $< 50\ \mu$m; axial *sniper-hole* protected by ceramic shutter.
- **Ignition drivers:** laser/coherent beams coupled through an axial port and/or peripheral pods; optics protected by sacrificial windows and segmented *shutters* (see Sec. **??**).
- **Sensors:** neutron fluxmeters, in-depth thermocouples, IR cameras, and particle detectors, integrated behind local shielding.

Conversion and cooling.

- **Primary: FLiBe** circuit in the NEH dome and backplate; transfer to a static heat exchanger through *step-and-dwell* coupling.
- **Secondary: Brayton/sCO_2** block with $\eta_{\text{el}} \approx 0.50$ (target regime with modern recuperators and turbomachinery).
- **Conservative case (wall-limited):** with $q_{\max} = 1.1$ MW/m^2 and base area

  $$A_{\text{hot}} = \frac{3\sqrt{3}}{2}s^2 \approx 2.598\ \text{m}^2 \quad (s = 1\ \text{m}),$$

  resulting in $q_{\max}A_{\text{hot}} \approx 2.86$ MW$_\text{t}$. With $\varepsilon_{\text{cap}} \sim 0.85$ and a transfer efficiency to cycle $\xi \sim 0.85$,

  $$P_{e,\text{cell}} \approx \varepsilon_{\text{cap}}\, \xi\, \eta_{\text{el}} \left(q_{\max}A_{\text{hot}}\right) \approx 0.85 \times 0.85 \times 0.46 \times 2.86 \approx \mathbf{0.94}\ \text{MW},$$

  which acts as the **design lower bound**.
- **Advanced option** (Appendix A): direct MHD conversion in variants with LiPb and dedicated B fields, with potential to increase $P_{e,\text{cell}}$ (at the cost of higher complexity).

Baseline MRFE (IGBI + higher cadence)

Fixing $Y_{\text{fus}} = 20$ MJ and $f_{\text{cell}} = 0.25$ Hz, with $\varepsilon_{\text{cap}} \approx 0.90$, $\xi \approx 0.90$, and $\eta_{\text{el}} \approx 0.50$, yields:

$$P_{e,\text{cell}} \;\approx\; Y_{\text{fus}}\, f_{\text{cell}}\, (\varepsilon_{\text{cap}}\, \xi\, \eta_{\text{el}}) \;\approx\; 20\text{ MJ} \cdot 0.25\text{ s}^{-1} \cdot 0.405 \;\approx\; \mathbf{2.03\ MW}.$$

The temporal deposition profile and the surface distribution of the dome keep peaks below $q_{\max}$. This value defines the *baseline* cell design in the standard operating regime of the MRFE.

Station topology and cadence calculation. The process ring incorporates multiple physical stations (N_{tot}), including: *injection/ignition*, *thermal extraction* (several), *staged cooling* (several), *inspection* (NDE, thermography, UT), and *maintenance* (cartridge/window swap). However, the sizing of dwell time per station and the per-cell cadence are fixed solely by the **thermally active** subset of stations, of size N_{th}, composed of: 1 for *injection/ignition* + N_{ext} for *heat extraction* + N_{cool} for *cooling*. *Inspection* and *maintenance* stations are executed in parallel or by diversion (bypass control), without penalizing the nominal production cycle.

$$N_{\text{th}} \;=\; 1 \;+\; N_{\text{ext}} \;+\; N_{\text{cool}}, \qquad t_{\text{dwell}} \;=\; \frac{1}{f_{\text{cell}}\, N_{\text{th}}}.$$

Baseline (production): we adopt $f_{\text{cell}} = 0.25$ Hz (1 shot/4 s) with $N_{\text{ext}} = 3$ and $N_{\text{cool}} = 2 \Rightarrow N_{\text{th}} = 6$, which sets the exact dwell:

$$t_{\text{dwell}} = \frac{1}{0.25 \times 6} = \frac{4\text{ s}}{6} = 0.667\text{ s}.$$

Typical physical stations: although $N_{\text{th}} = 6$ governs cadence, the ring integrates $N_{\text{tot}} \approx$ 10–12 stations, e.g.:

- 1 for *injection/ignition*;
- 3 for *IGBI extraction* (fixed exchangers with He *impinging jets*);
- 2 for *staged cooling* (thermal polishing and equalization);
- 2 for *inspection* (thermography/UT, structural and optical health);
- 1–2 for *maintenance* (cartridge/window swap) via bypass.

Control margin: under a thermal protection order or process transient, the controller can temporarily extend the dwell of a station up to $t_{\text{dwell,max}} = 1.0$ s. If this value were applied in *all* thermal stations of a cycle, the effective cadence would drop to $f_{\text{cell,eff}} = \frac{1}{N_{\text{th}}\, t_{\text{dwell,max}}} \approx 0.167$ Hz. The supervisor gradually restores the nominal value (0.25 Hz) in subsequent cycles.

Maintenance and interchangeability.

- **Integrated cartridge** (Dome + hot-plate + NEH) with robotic extraction/insertion; typical replacement due to fatigue/irradiation every 1–3 years (see Sec. 4.6).
- **Windows/shutters** *hot-swappable* at station, multiplexing ports to minimize *downtime*.
- **Interfaces:** flanges with metallic C-seal, *dry-breaks* and He purge; micrometric re-alignment at *dock*.

Table 1: Critical materials of the reference cell module and indicative properties

Material	Density [g/cm^3]	k [W/mK]	R_{yield} [MPa]	Main function
RAFM (steel)	7.8–7.9	20–30	500–650	Structure/backplate, manifolds
W–SiC (cermet)	10–14 (eff.)	80–150	400–600	PFC/tiles in *hot-plate* and dome
FLiBe (liq.)	1.9–2.1	1–2	–	Breeding and primary cooling
B_4C (layer)	2.5	15–30	–	Neutron thermal absorption
Graphite/SiC	1.8–3.2	120–200	–	Thermal diffusion, selective liners
He (IGBI)	1.6×10^{-4}	0.15	–	*Impingement* + thermal recovery

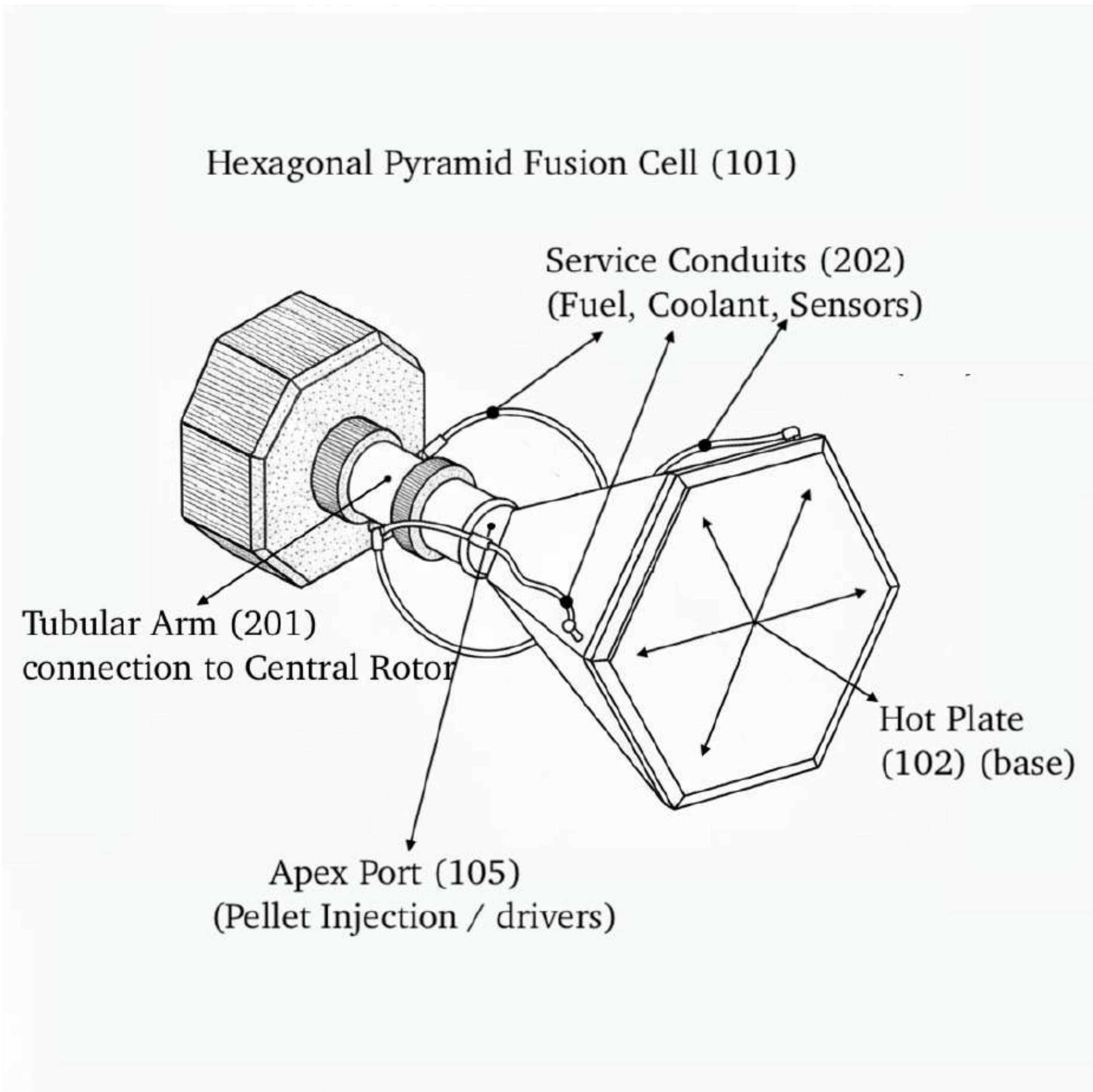

Figure 1: Fusion cell with truncated hexagonal NEH dome, collimated optical ports, and hot-plate cartridge. The apex vertex of the pyramid connects through channels to the rotor, serving as a bus for multiple functions.

4.1.1 Energy Balance per Cell and Calibration

Objective. To establish the energy balance per *cell* (hexagonal pyramid, $s = 1$ m side length) as the basic design unit, **calibrated solely with the NEH dome and IGBI interface**, and usable for direct scaling to any rotor.

Per-shot definitions.

$$\begin{aligned}
E_L &: \text{driver energy coupled to the target [J]}, && (1)\\
E_{\text{fus}} &: \text{fusion energy per shot [J]}, \quad G \equiv E_{\text{fus}}/E_L, && (2)\\
\eta_{\text{drv}} &: \text{driver wall–plug efficiency}, && (3)\\
\varepsilon_{\text{cap}} &: \text{fraction of } E_{\text{fus}} \text{ captured by NEH dome + hot-plate}, && (4)\\
\xi &: \text{thermal transfer efficiency (IGBI} \to \text{cycle)}, && (5)\\
\eta_{\text{el}} &: \text{thermal}\to\text{electric efficiency (Brayton/sCO}_2\text{)}, && (6)\\
f_{\text{cell}} &: \text{per-cell firing rate [Hz]}, \quad d: \text{ duty cycle}, \quad f_{\text{eff}} = d\, f_{\text{cell}}. && (7)
\end{aligned}$$

Average power (per cell).

$$\begin{aligned}
P_{\text{fus,cell}} &= f_{\text{eff}}\, E_{\text{fus}}, && (8)\\
P^{(\text{el})}_{\text{out,cell}} &= P_{\text{fus,cell}}\, (\varepsilon_{\text{cap}}\, \xi\, \eta_{\text{el}}), && (9)\\
P^{(\text{drv})}_{\text{in,cell}} &= \frac{f_{\text{eff}}\, E_L}{\eta_{\text{drv}}} = \frac{f_{\text{eff}}\, E_{\text{fus}}}{G\, \eta_{\text{drv}}}, && (10)\\
P_{\text{net,cell}} &= P^{(\text{el})}_{\text{out,cell}} - P^{(\text{drv})}_{\text{in,cell}} - P_{\text{aux,cell}}, && (11)
\end{aligned}$$

with feasibility condition:

$$G\, (\varepsilon_{\text{cap}}\, \xi\, \eta_{\text{el}}) \; > \; \frac{1}{\eta_{\text{drv}}}.$$

Reference architecture and materials (consistent with Sec. 4.6).

- **Structure:** casing and edges in **RAFM steel** with lattice stiffeners (WAAM/HIP).
- **Hot-plate: W–SiC** tiles (15–25 mm) over **RAFM backplate** (25–30 mm).
- **NEH dome** (integrated cartridge): W–SiC PFC (20–30 mm) + **FLiBe** microchannels (60–80 mm) + **B_4C** (5–10 mm) + **RAFM** back-plate (20–30 mm).
- *Option* (Appendix A): LiPb variants with direct MHD conversion.

Wall thermal limits.

- Admissible wall heat flux (hot zone): $q_{\text{max}} \approx 1.1$ MW/m^2 (conservative W–SiC PFC design).
- Wall temperature: $T_{\text{wall}} \leq 1200$ K nominal, with short excursions up to ~ 1400 K.

Calibration (baseline IGBI). With IGBI interface (pressurized He impinging jets + high-conductivity pin–fins) and Brayton/sCO_2 cycle, we adopt:

$$Y_{\text{fus}} = E_{\text{fus}} = 20\ \text{MJ/shot}, \quad f_{\text{cell}} = 0.25\ \text{Hz}, \quad \varepsilon_{\text{cap}} \approx 0.90,\ \xi \approx 0.90,\ \eta_{\text{el}} \approx 0.50.$$

Thus:

$$P_{\text{fus,cell}} = 20\ \text{MJ} \times 0.25\ \text{s}^{-1} = 5.0\ \text{MW}, \qquad P^{(\text{el})}_{\text{out,cell}} = 5.0 \times (0.90 \times 0.90 \times 0.50) \approx \mathbf{2.03\ MW}.$$

Hence we adopt $\boxed{P^{\text{net}}_{\text{cell}} \simeq \mathbf{2.03\ MW}}$ as the **design value** (plant parasitics treated at rotor/plant level).

Operating range. For $\{Y_{\text{fus}}, f_{\text{cell}}\} = \{15\text{–}25\ \text{MJ},\ 0.20\text{–}0.25\ \text{Hz}\}$ with the same efficiencies,

$$P^{(\text{el})}_{\text{out,cell}} \in [1.35,\ 2.25]\ \text{MW},$$

with the upper bound further *capped* by $q_{\max} A_{\text{hot}}$ (Sec. 4.1).

Annual production per cell. With availability $u = 95\%$:

$$E_{\text{year,cell}} = P^{\text{net}}_{\text{cell}} \times 8760\ \text{h} \times u \ \approx\ 2.03 \times 8760 \times 0.95 \ \approx\ \mathbf{16.9}\ \text{GWh/year}.$$

(For energy pricing and margins, see Sec. 5.)

Parameter	**Design value**	**Operating range**
Cell size (side s)	1.0 m	–
Admissible heat flux $q_{\max}$	1.1 MW/m^2	1.0–1.2 MW/m^2
Hot-plate (W–SiC + RAFM)	15–25 mm + 25–30 mm	–
NEH dome (PFC + FLiBe + B_4C + RAFM)	20–30 + 60–80 + 5–10 + 20–30 mm	–
Cell cadence f_{cell}	0.25 Hz	0.20–0.25 Hz
Electric power per cell	**2.03 MW**	1.35–2.25 MW
Annual output (u=95%)	**16.9 GWh/year**	11.2–18.8 GWh/year

Technical summary table.

Note on drivers. The condition $G(\varepsilon_{\text{cap}}\xi\eta_{\text{el}}) > 1/\eta_{\text{drv}}$ sets the admissible pair (G, η_{drv}) for the baseline. Driver power and other electric parasitics are consolidated at the *rotor/plant* level (Sec. 4.2 and Sec. 5), while here the calibration remains at the cell thermal–electric level.

4.1.2 Cell Durability and Maintenance

Objective. To ensure that each cell can operate in repetitive regime with minimal interruption, defining quantitative criteria for preventive replacement and robotic substitution procedures.

Typical replacement sequence (robotized).

1. Hydraulic isolation and He purge of the NEH cartridge.
2. Removal of auxiliary power and mechanical lock of the anchor.
3. Disconnection of hydraulic *dry-breaks* (auto-sealing) and docking electrical connector.
4. Automated unscrewing of anchors by torque-controlled robots.
5. Extraction using telescopic *dolly* and transfer to maintenance/storage cell.
6. Insertion of new cartridge and verification of flatness, leak-tightness (He leak-test $< 10^{-9}$ mbar·L/s) and realignment.

Target times.

- Robotized cartridge swap time: < 15 min (design with 2 redundant robots).
- Inline rapid inspection (thermography + UT): < 5 min per cartridge.
- Optical window/shutter *hot-swap*: ≤ 2 min.

Replacement frequency criteria. Cartridge lifetime is defined as the minimum among the following limits, applying a safety factor $SF \simeq 0.7$:

- **Thermo–mechanical fatigue (backplate, RAFM).** Coffin–Manson–Basquin model with $\Delta T \sim$ 150–200 K per shot, $\alpha \approx 12 \times 10^{-6}$/K, $E \sim 200$ GPa. Typical lifetime: $N_f \sim 10^5$–3×10^5 cycles. $\Rightarrow$ replacement every 1–3 years at $f = 0.25$ Hz (1 shot/4 s).
- **Irradiation (DPA).** Thresholds: W (5–10 dpa), RAFM (10–20 dpa). For flux $\phi_n \sim 10^{18}$ n/m^{2}s on the first wall:
$$\text{DPA/year} \sim 5-10, \quad t_{\text{DPA}} \sim 1-3 \text{ years.}$$
- **Erosion/corrosion.** Sputtering in W: $\Delta x \sim 0.01$ mm/year. Corrosion in FLiBe: 0.05–0.1 mm/year (uncoated); < 0.01 mm/year with SiC/Al_2O_3 coatings. Estimated lifetime > 20 years $\Rightarrow$ not governing.
- **Optics and sensors (ports).** Transmittance decays as
$$\mathcal{T}(n) = \mathcal{T}_0 \, e^{-\beta n}, \qquad n_{0.9} \approx \frac{0.1053}{\beta},$$
with $\beta \sim 10^{-6}$–10^{-5}/shot. Typical lifetime 10^4–10^5 shots. With multiplexing $m = 3-4$ and $f = 0.25$ Hz $\Rightarrow T \sim 7$–19 days. Hot-swap in 2 min $\Rightarrow$ downtime $< 0.03\%$.

Limit	Key variable	Model	Typical lifetime	Govern
Thermo–mechanical fatigue (RAFM)	$\Delta T, f$	Coffin–Manson	1–3 years	Ye
Irradiation (DPA)	Fluence, dpa/year	Threshold 10–20 dpa	1–3 years	Ye
W erosion (PFC)	Y, Φ	Rate mm/year	20–40 years	No
FLiBe corrosion	mm/year	Mitigated by SiC	20–50 years	No
Optics/windows (with m)	β, f, m	$\mathcal{T}(n)$ and $T = \frac{Nm}{f}$	7–19 days (ex.: f=0.25 Hz, m=3–4) downtime $< 0.03\%$	No

Table 2: Estimated lifetime criteria for the NEH+dome+hot-plate cartridge and its ports.

f (Hz)	m	N (shots)	T (days)	t_{swap} (min)	downtime
0.25	2	5×10^4	4.63	2	0.030%
0.25	3	5×10^4	6.94	2	0.020%
0.25	4	5×10^4	9.26	2	0.015%
0.25	4	1×10^5	18.52	2	0.0075%

Table 3: Sensitivity of replacement interval $T = \frac{Nm}{f}$ and downtime $\approx t_{\text{swap}}/T$.

Synthesis.

- The dominant lifetime limits are **thermo–mechanical fatigue** and **irradiation**, imposing cartridge replacement every 1–3 years.
- Corrosion/erosion is not governing for horizons < 10 years if protective coatings are applied.
- Optics/windows require frequent replacement, but with *multiplexing* and *hot-swap* the impact on availability is negligible.

Recommended frequency.

- **NEH+hot-plate cartridge:** replacement every 1–3 years at $f = 0.25$ Hz; annual NDE inspection.
- **Complete module (dome+NEH+hot-plate):** major replacement every 5–7 years.

Integration note. The detailed description of dome NEH geometry, layers, and architecture is developed in Sec. 4.6. Complete cartridge swap and maintenance procedures are further expanded in Sec. 4.10, covering the cell level and the integrated replacement system.

4.2 Rotor Energy Balance

Objective. To calibrate the net power and energy of a rotor from the net power per cell, and to set the *Minimum Viable Product (MVP)* as the minimum number of cells that yields a **positive economic surplus** (after amortization and OpEx), together with a *Functional Reference Rotor (FRE)* serving as a replicable design point.

Reference parameters per cell. Baseline scenario (Sec. 4.1): performance per cell

$$P_{e,\text{cell}} = \mathbf{2.03}\ \text{MW}, \qquad Y_{\text{fus}} = 20\ \text{MJ},\ f_{\text{cell}} = 0.25\ \text{Hz},\ \varepsilon_{\text{cap}} \approx 0.90,\ \xi \approx 0.90,\ \eta_{\text{el}} \approx 0.50.$$

Operational availability $u = 95\%$ and average selling price $\pi = \mathbf{75.9}$ /MWh.

Power and energy per rotor with N cells.

$$P_{e,\text{rotor}}(N) = N\, P_{e,\text{cell}}, \tag{12}$$

$$E_{\text{year}}(N) = P_{e,\text{rotor}} \times 8760\,\text{h} \times u. \tag{13}$$

Annual revenues:

$$\text{Revenue}(N) \;=\; E_{\text{year}}(N) \times \pi.$$

MVP criterion (economic, conservative). We define MVP as the minimum N such that the **annual net surplus** per rotor is positive:

$$\text{Surplus}(N) \;=\; \text{Revenue}(N) \;-\; \underbrace{N\,\text{CapEx}_{\text{cell}}/T_{\text{amort}}}_{\text{annual amortization}} \;-\; \underbrace{N\,\text{OpEx}_{\text{cell}}}_{\text{operation and maintenance}} \;-\; \text{OpEx}_{\text{common}} \;>\; 0,$$

with conservative assumptions (no MHD, FLiBe, RAFM/W–SiC, WAAM/HIP):

$$\text{CapEx}_{\text{cell}} \in [4.0, 5.0]\ \text{M}, \quad T_{\text{amort}} = 10\ \text{years}, \quad \text{OpEx}_{\text{cell}} \approx 0.15\ \text{M/year}, \quad \text{OpEx}_{\text{common}} \approx 0.5\ \text{M/year}.$$

With $P_{e,\text{cell}} = 2.03$ MW and $\pi = 75.9$ /MWh, the **revenue per cell** is:

$$\text{Revenue}_{\text{cell}} \;=\; 2.03 \times 8760 \times 0.95 \times 75.9 \;\approx\; \mathbf{1.28}\ \text{M/year}.$$

Amortization + OpEx per cell $\approx (0.40\text{–}0.50) + 0.15 = 0.55\text{–}0.65$ M/year, hence the **margin per cell** is $\sim 0.63\text{–}0.73$ M/year. Thus, the condition of positive surplus is met comfortably starting from $\mathbf{N = 18}$ (see table).

Config.	Cells N	$P_{e,\text{rotor}}$ [MW]	E_{year} (95%) [GWh]	Revenue (95%) [M€/year]
MVP (min. surplus >0)	**18**	36.54	304.1	23.08
FRE (functional reference)	**24**	48.72	405.4	30.77
32 cells	32	64.96	540.6	41.01
48 cells	48	97.44	810.9	61.52
60 cells	60	121.8	1,014.	76.89

Table 4: Rotor power, annual energy (with $u = 95\%$) and revenue at $\pi = 75.9$ / MWh for different N.

Technical–economic reading.

- With the baseline $P_{e,\text{cell}} = 2.03$ MW, the **economic MVP** is reached at **18** cells, leaving a margin above amortization+OpEx under conservative assumptions.
- The **reference rotor (FRE)** with $N = 24$ cells delivers ~ 48.7 MW net and ~ 405 GWh/year, with revenues of ~ 30.8 M/year.

- Scaling N is linear in both power and revenues; the optimal decision will be made against available CapEx, operational risk, and plant ramp-up strategies (Sec. 5).

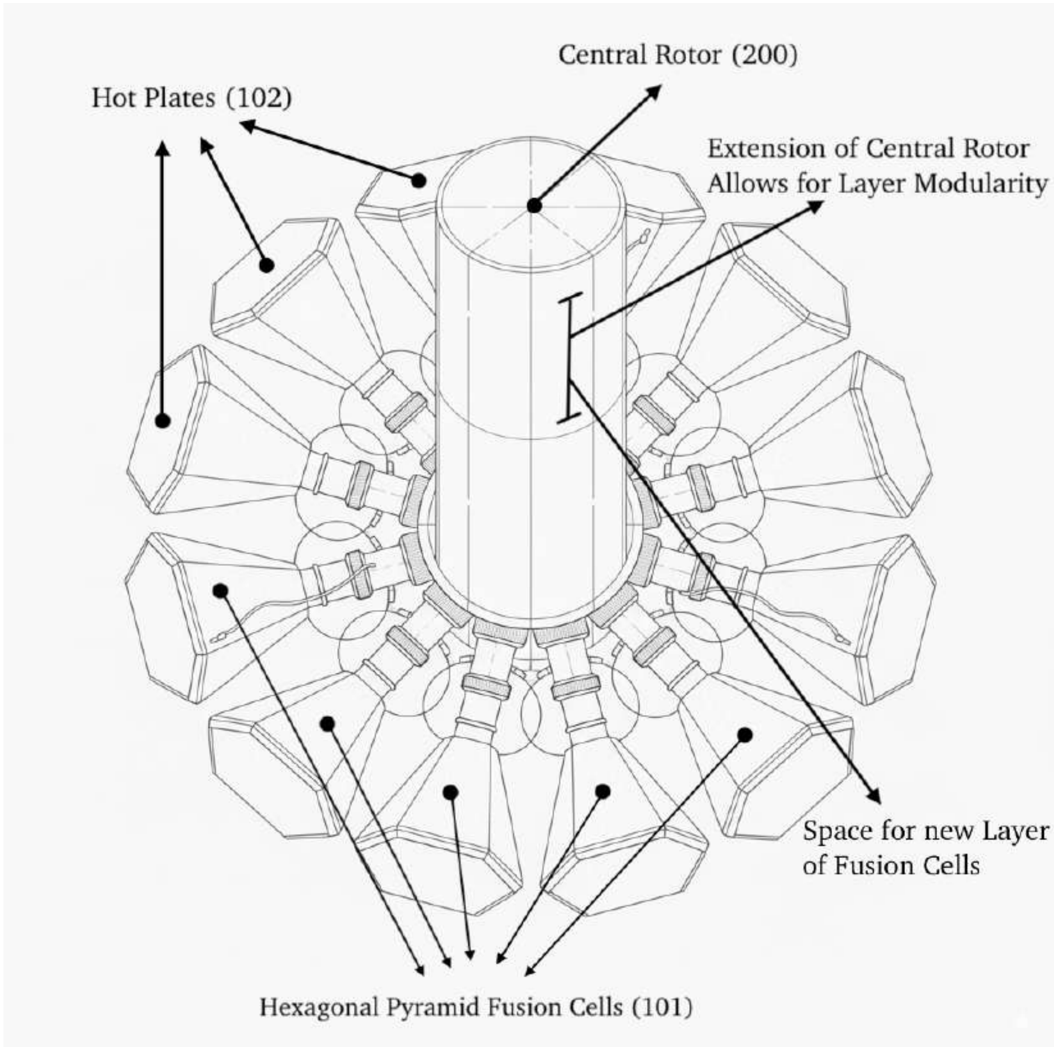

Figure 2: Extended central rotor with 12 coupled fusion cells. The modular architecture —both of the rotor and the cells— allows the design to be extended to include additional layers of cells, enabling a wide variety of configurations. Modularity is only limited by the diameter and length of the central rotor, admitting more or fewer cells and ring-layers accordingly.

4.3 Rotor "tick" architecture (12 stations, 2 ignition points)

Each rotor revolution is discretized into **12 stations** with fixed **dwell time per station**

$$t_{\text{dwell}} = \mathbf{0.67\ s} \quad \text{(control with admissible variance up to 1.0 s under contingency)},$$

and **2 diametrically opposed ignition stations**. The kinematic magnitudes are defined as:

$$T_{\text{rev}} = N_{\text{est}}\, t_{\text{dwell}} = 12 \times 0.67 = \mathbf{8.04\ s}, \qquad \text{rpm} = \frac{60}{T_{\text{rev}}} = \mathbf{7.46\ rpm}.$$

The **per-cell cadence** is

$$f_{\text{cell}} = \frac{N_{\text{ign}}}{N_{\text{est}}\, t_{\text{dwell}}} = \frac{2}{12 \times 0.67} = \mathbf{0.25\ Hz} \quad \text{(1 shot every 4 s per cell)}.$$

Note: f_{cell} depends only on $(N_{\text{est}}, N_{\text{ign}}, t_{\text{dwell}})$ and is **independent** of the total number of rotor cells; the number of cells scales the total power, not the cadence of each cell.

Station map (functional example).

#	Station	Main function
1	Ignition A	Firing + faceted shutter closure
2	IGBI–1	Hot discharge (impinging He + TZM pin-fins)
3	IGBI–2	Hot discharge (second stage)
4	Pre–He–1	Pressurized helium convection (polishing 1)
5	QA–1	Thermography, fluxmeters, pose verification
6	Service	Service window: purges, micro-adjustments, optical *hot-swap* if required
7	Ignition B	Diametral firing
8	IGBI–3	Hot discharge (third stage)
9	IGBI–4	Hot discharge (fourth stage)
10	Pre–He–2	Pressurized helium convection (polishing 2)
11	QA–2	Secondary inspection and validation
12	Buffer/Bypass	Operational margin (latency, synchronization, brief contingencies)

Integration with the thermal cycle. The four IGBI stages (Stations 2,3,8,9) manage the pulse in a staggered manner, limiting $\Delta T/\Delta t$ at the hot-plate and keeping useful flux under the design threshold q_{max}; the pre-cooling stages (Stations 4 and 10) stabilize the wall at ∼600–800 K prior to QA/Service.

Kinematic summary (baseline by ticks)

$$\boxed{\begin{aligned} &N_{\text{est}} = 12, \quad N_{\text{ign}} = 2, \quad t_{\text{dwell}} = 0.67\ \text{s}, \\ &T_{\text{rev}} = 8.04\ \text{s}, \quad \text{rpm} = 7.46, \quad f_{\text{cell}} = 0.25\ \text{Hz}. \end{aligned}}$$

The *step–and–dwell* control accepts temporal variance per station up to 1.0 s under contingency, with automatic replanning to preserve the mean value of f_{cell}.

4.4 Operating Cycle and Performance (architecture with NEH dome)

Each fusion cell follows a repetitive cycle of *fuel loading* $\rightarrow$ *ignition* $\rightarrow$ *energy collection* $\rightarrow$ *staged cooling* $\rightarrow$ *reload*. The rotating assembly and temporal staggering between cells ensure that the rotor delivers **essentially continuous power**.

Reference assumptions per cell

- Geometry: hexagonal pyramid ($s \approx 1.0$ m, $A_{\text{hot}} \approx 2.60$ m^2) with **NEH dome** coupled to the base.
- Cryogenic D–T target; fusion energy per shot $\mathbf{E}_{\text{fus}} = \mathbf{20}$ MJ.
- Capture/conversion: $\varepsilon_{\text{cap}} \approx 0.90$, transfer efficiency to cycle $\xi \approx 0.90$, and thermal-to-electric efficiency $\eta_{\text{el}} \approx 0.50$ (Brayton sCO_2 with recuperator). *No MHD in the baseline* (see Appendix A for options).
- Thermal interface at station: **IGBI** (pressurized He impinging jets + high-conductivity *pin–fins*/"forest") in a controlled gap ($\sim$0.5–1.0 mm), with $h_{\text{eff}} \sim$ 6,000–9,000 W m^{-2}K^{-1}.
- Cadence: $\mathbf{f}_{\text{cell}} = \mathbf{0.25}$ Hz (one ignition/4 s); cell availability $u = 95\%$.
- Net power per cell (calibrated): $\mathbf{P}_{\text{cell}}^{\text{net}} \approx \mathbf{2.03}$ MW.

Validated baseline (per cell)

$Y_{\text{fus}} = 20$ MJ, $f_{\text{cell}} = 0.25$ Hz, $\varepsilon_{\text{cap}} = 0.90$, $\xi = 0.90$, $\eta_{\text{el}} = 0.50 \;\Rightarrow\; P_{e,\text{cell}} \approx Y_{\text{fus}}\, f_{\text{cell}}\,(\varepsilon_{\text{cap}}\xi\eta_{\text{el}}) = 20 \cdot 0.25 \cdot 0.405 \approx \mathbf{2.03}$ MW.

(i) Fuel loading.

- D–T pellets (sub-mg to mg) stored cryogenically.
- Axial injection with alignment $< 50\ \mu$m and velocity 100–200 m/s (see Sec. **??**).
- Pre-optical verification and phase synchronization (*jitter* < 10 ps).

(ii) Ignition.

- Drivers: cluster of Nd:glass lasers (351 nm) with redundancy and thermal load sharing.
- Pulse: coupled energy E_L to achieve nominal $E_{\text{fus}} = 20$ MJ.
- Species: $\sim$80% neutrons at 14.1 MeV, $\sim$20% α particles at 3.5 MeV.

(iii) Energy collection and pathways.

- Interception dome+plate: the NEH dome and multilayer base absorb $\varepsilon_{\text{cap}} \approx 0.90$ of E_{fus}.
- Thermal conversion: **FLiBe** in dome/backplate $\rightarrow$ recuperative heat exchanger $\rightarrow$ Brayton sCO_2 cycle with $\eta_{\text{el}} \approx 0.50$ (baseline without MHD).
- Tritium breeding: ^{6}Li(n,α)T in FLiBe (regeneration fraction $\sim$ 20%, see Sec. **??**).
- Shielding: the dome attenuates flux toward the apex, extending optics and sensor lifetime.

(iv) Staged cooling and *step-and-dwell*. The cycle scheduler defines **6 temporal slots** per shot (total 4.0 s), with exact dwell $\mathbf{t}_{\text{dwell}} = \mathbf{0.667}$ s per slot. Control admits extension up to 1.0 s under contingency (e.g., thermal stabilization). The *physical stator stations* are ≥ 9 (injection/ignition, 3–4 thermal IGBI, 2 deep cooling, inspection/QA, maintenance 1 and 2); not all are visited in every shot.

1. **S0:** injection+ignition (aligned with apex port).
2. **S1–S3:** thermal extraction IGBI (He jets 6–9 bar + *pin–fins*, $h_{\text{eff}} \sim$ 6–9 kW/m^{2}K).
3. **S4:** deep cooling / recuperator (wall $\to \sim$ 600–700 K).
4. **S5:** service window (quick inspection, QA); maintenance stations scheduled on demand.

(v) Net energy per shot (consistency check).

$$E_{\text{shot,el}} = \frac{P_{\text{cell}}^{\text{net}}}{f_{\text{cell}}} = \frac{2.03}{0.25} \approx 8.1 \text{ MJ}, \quad 20 \text{ MJ} \times 0.90 \times 0.90 \times 0.50 \approx 8.1 \text{ MJ}.$$

Table 5: Net production with NEH dome and IGBI interface (baseline $P_{\text{cell}}^{\text{net}} \approx 2.03$ MW).

Configuration	N (cells)	$P_{\text{rotor}}^{\text{net}}$ [MW]	E_{year} (95%) [GWh]	Notes
FRE (24 cells)	24	48.7	405	Functional reference
Medium scale	40	81.2	676	Higher modularity
High platform	60	121.8	1,014	Full plant

(vi) Rotor operation scenarios (baseline without MHD).

(vii) Fault tolerance and lifetime.

- Ignition failure: loss $< 4.2\%$ (FRE, 24 cells); in 60 cells, $\sim 1.7\%$.
- NEH+hot-plate cartridge: replacement every 1–3 years ($\sim 10^5$ cycles); NEH dome longer lifetime (5–7 years).
- Multiplexing and optical *hot–swap* minimize downtime ($< 0.05\%$).

4.5 NEH Blanket and Integration

The pyramidal walls (103) surrounding the fusion cavity form a **multilayer Neutron Energy Harvesting (NEH) blanket**. Each layer is designed to sequentially absorb, moderate, and convert the 14 MeV neutron flux, while breeding tritium, extracting high-temperature heat, and providing structural integrity.

Reference stack (baseline).

1. **Plasma-facing layer (20–25 mm):** sintered W–SiC tiles. Functions:
   - Resistance to thermal shocks $> 10^7$ W/m^2.
   - Capture of α particles (3.5 MeV, ∼20% of E_{fus}).
   - Primary shielding against X-rays and charged particles.
2. **Moderator/multiplier (30–40 mm):** Be/BeO blocks interleaved with SiC. Functions:
   - Moderation of neutron spectrum from 14 MeV to 0.1–1 MeV (optimal for ^{6}Li capture).
   - Neutron flux multiplication via (n,2n) reactions in ^{9}Be.
   - Thermal diffusion and gradient buffering.
3. **Breeder/coolant (60–80 mm):** liquid **FLiBe** (^{6}LiF–BeF$_2$). Functions:
   - Tritium breeding via ^{6}Li(n,α)T ($\sigma \sim 940$ barns).
   - Heat extraction at 700–800°C for sCO$_2$ Brayton cycle.
   - Compatibility with SiC coatings to minimize corrosion/erosion.
   - Optional B$_4$C laminates (2–3 mm) to capture residual neutrons.
4. **Structural/back plate (20–30 mm):** RAFM ferritic–martensitic steel (e.g., EUROFER97). Functions:
   - Mechanical support of the modular cartridge.
   - Integration of cooling microchannels and manifolds for extraction to exchangers.

Thermal conversion path (baseline). Captured heat is conducted to a **closed Brayton cycle** with supercritical CO$_2$, with efficiency $\eta_{\text{el}} \sim 0.45$–$0.50$ under nominal operation. This value is adopted as the **reference efficiency** for rotor sizing.

Advanced option (Appendix A). In alternative configurations with eutectic LiPb (17Li–83Pb), breeder channels may also function as MHD conduits under a dedicated $B \sim 5$ T field. This would enable direct electrical conversion with additional efficiency $\eta_{\text{MHD}} \sim 5$–10%, albeit at the cost of greater technological complexity.

Modular shielding and replacement. The hot plate coupled to the NEH radiator is implemented as a **removable cartridge**, total thickness $t_{\text{plate}} \sim 20$–30 cm:

- Robotized replacement every $\sim 10^5$ cycles (≈ 1.5 years at nominal cadence).
- Independent dome vs. plate replacement, reducing costs and downtime.
- Modular architecture: local erosion or point activation does not compromise the entire cell.

4.6 Detailed Architecture of the NEH Dome: Truncated Hexagonal Prism (Specifications)

This subsection develops the construction aspects of the *NEH Dome* and its integration into a **removable integrated module** (MIDH: Dome + Hot-plate + NEH). While Sec. 4.1.2 establishes *lifetime and replacement criteria* at the cell level, here the **physical and engineering characteristics** of the cartridge are detailed: geometry, layer stack, mechanical, hydraulic and electrical interfaces, as well as thermal budget and mass estimates.
Throughout the document the following nomenclature is used:

- *NEH blanket*: the global neutron energy extraction and conversion system of the plant.
- *Lateral NEH cartridge*: removable modular unit on rails, including breeder+moderator+internal structures (1–2 year replacement).
- *Integrated Dome–HotPlate–NEH Module (MIDH)*: also termed *Modular Removable Base (BEM)*, grouping the dome, hot-plate and full NEH (5–7 year replacement).

4.6.1 Macroscopic geometry

- **Type:** truncated hexagonal prism (hexagonal base, six inclined faces, upper truncation).
- **Base side:** $s = 1.00$ m, base area $A_{\text{hot}} = \frac{3\sqrt{3}}{2}s^2 \approx 2.60$ m^2.
- **Internal height:** $H_{\text{dome}} = 0.22$ m (range 0.18–0.25 m).
- **Upper truncation:** coaxial hexagon $s_{\text{top}} = 0.25$ m with central axial port.
- **Back plate (dorsal):** $t_{\text{dorsal}} = 20$ mm RAFM/ODS (15–25 mm).

4.6.2 Ports and "sniper-holes"

Central axial port (injection/diagnostics):

- Internal diameter: $\varnothing$100 mm (industrial standard criterion).
- W liner 6 mm; faceted *shutter* with diaphragm-type opening (< 5 ms).
- Coaxial axis tolerance < 100 μm.

Peripheral ports (auxiliary optics):

- Number: 6 (one per face), inclination 12°–18°.
- Diameter: $\varnothing$40–50 mm, W liner 3–5 mm.
- Labyrinth slot + local He purge.

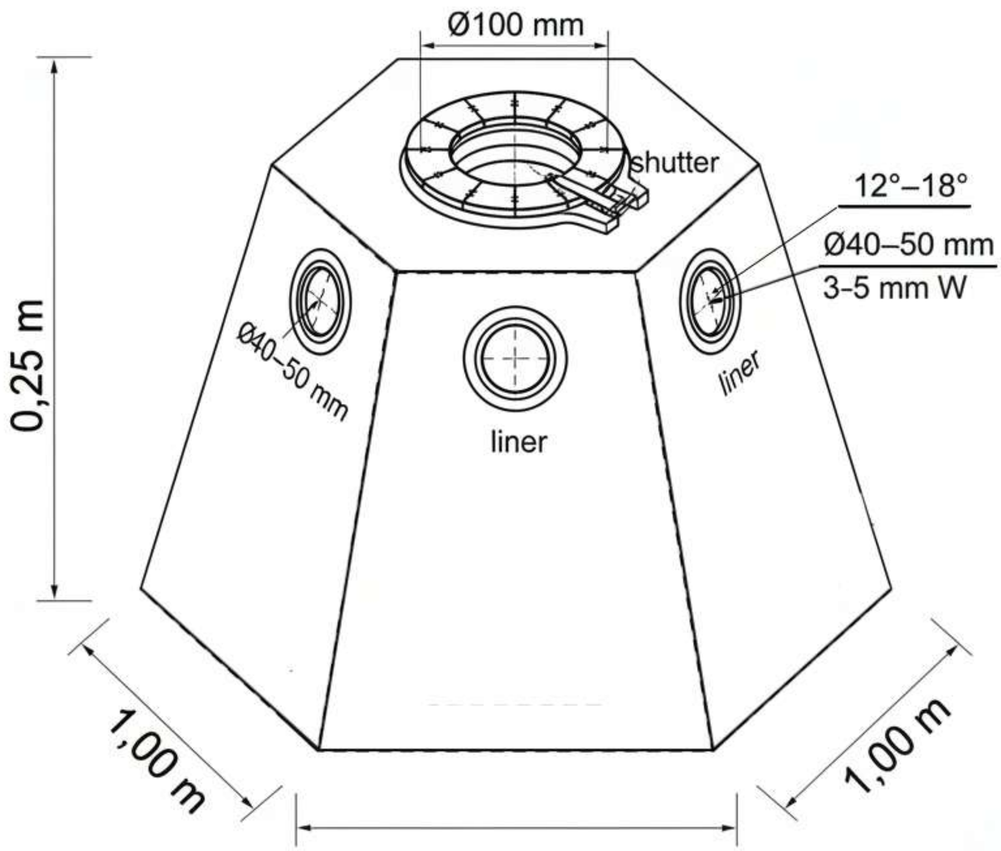

Figure 3: Technical schematic of the **truncated prism NEH Dome**, showing geometry and nominal dimensions: base side $s = 1.0$ m, height $H = 0.25$ m, central axial port $\oslash 100$ mm with fast-closing *faceted shutter* (< 5 ms), and six peripheral ports $\oslash 40$–50 mm (inclination 12–18°), equipped with tungsten liners (3–5 mm). The design ensures compatibility with coaxial and peripheral laser beams while minimizing radiative leakage during operation.

4.6.3 Layer stack

1. **PFC (plasma-facing component):** W or W–SiC, $t = 40$ mm.
2. **Moderator/multiplier:** Be/BeO + C/SiC layers, $t = 30$ mm.
3. **Breeder/coolant:** FLiBe (enriched ^{6}Li), $t = 70$ mm, with radial microchannels.
4. **Absorber:** B_4C or Gd_2O_3, $t = 8$ mm.
5. **Back-plate:** RAFM/ODS, $t = 20$ mm, with secondary cooling microchannels.

Nominal total thickness: $t_{\text{dome,tot}} \approx 168$ mm.

4.6.4 IGBI system (Gas–Brush Impingement Interface)

Concept. The IGBI system constitutes a specific invention of the MRFE: a thermal dissipation interface based on *pressurized helium impinging jets* (6–10 bar) onto a **forest of metallic pin–fins** manufactured in TZM alloy. This metallic forest is diffusion-welded to the hot-plate, ensuring homogeneous thermal conductivity.

Technical characteristics.

- **Pins:** TZM cylinders, diameter 1–2 mm, height 5–10 mm, surface density $> 5000/\text{m}^2$.
- **Integration:** monomaterial block (TZM), diffusion-welded to the backplate.
- **Helium flow:** convective coefficient $h > 15{,}000$ W/m^{2}K in pulsed regime.
- **Heat removal capacity:** $>$ 10 MW per station, well above requirements.

Overdimensioning. The IGBI is designed with ample margin: even if Y_{fus} increases up to 25–30 MJ per shot, its thermal removal capacity exceeds the deposited energy. This enables a **future scaling option** without redesigning the thermal interface.

4.6.5 Thermal budget and limits

- Allowable wall flux: $q_{\text{allow}} = 1.0\text{–}1.2$ MW/m^2.
- Energy absorbed by hot-plate per shot: $E_{\text{dep}} \approx 4\text{–}6$ MJ.
- PFC thermal peak: $T_{\text{peak}} \sim 1500\text{–}1700$ K, $\Delta T \sim 200$ K.

4.6.6 Integrated module (MIDH / BEM)

- **Lateral NEH cartridge:** 1.5–2.0 t, replacement every 1–2 years.
- **Complete MIDH module:** 3.5–4.5 t, replacement every 5–7 years.
- **Advantage:** massive extractions are minimized, critical materials remain confined, and overall rotor availability remains high.

4.6.7 Functional summary

- The prismatic dome increases neutron capture fraction by +15–20%.
- The IGBI system constitutes a **key innovation**, capable of removing > 10 MW without redesign, allowing Y_{fus} scaling.
- Modularity (lateral cartridge vs. full MIDH) provides logistical flexibility and economic resilience.

4.7 Risks and mitigations: thermo–mechanical fatigue, coupling alignment, and vibration control

(i) Thermo–mechanical fatigue and differential expansion. The joints between the integrated cartridge (Dome+NEH+Hot–plate) and the supporting ring undergo cyclic thermal gradients (dome $\sim 800°$C vs. ring/arms at 400–500°C), generating alternating stresses $\Delta\sigma$ and risk of low-cycle fatigue damage accumulation. The invention mitigates this by:

- **Isothermal ring:** the rotor ring is maintained at a stable setpoint T_{ring} through *reverse heat recirculation*: a closed He/CO_2 loop redistributes surplus heat from NEH-coupled radiators to channels embedded in the ring. Trace resistors (NiCr) correct deviations under PID control, limiting $\Delta T_{\text{cell-ring}} < 40°$C.
- **Kinematic and compliant mounts:** three-point supports with spherical pads + Ti/INVAR laminates absorb $\Delta L = \alpha L \Delta T$ without over-restriction; dry MoS_2/graphite coatings limit stick–slip.
- **Low-CTE inserts and graded transitions:** W–SiC/RAFM transitions in the dome backplate reduce CTE mismatch with the Ti–6Al–4V ring.
- **Safe fatigue sizing:** alternating stresses at critical points kept $< 0.4\,\sigma_y$ at setpoint. Miner/ASME VIII rules satisfy $\sum n_i/N_i < 0.2$ for lifetime $\geq 10^5$–3×10^5 cycles (∼1–3 years at 0.25 Hz, see Sec. 4.1.2).

(ii) Coupling alignment and clearance control. Thermal discharge from the integrated cartridge to the IGBI radiator requires coplanarity and millimetric clearance control to ensure reproducible coupling without mechanical wear.

- **Optical alignment:** laser fiducials + quadrant photodiodes at discharge stations, with CMOS triangulation for validation. Tolerances: flatness < 100 μm, lateral < 150 μm, axial clearance 0.5–1.5 mm, critical to ensure uniform He jet impingement at the IGBI.
- **Kinematic couplers:** wedge/sphere contacts define deterministic position. Flexures (1–2 mm) absorb micro-errors while maintaining uniform pressure.
- **Actuated micro-stages:** piezoelectric (±250 μm) correct residual deviations before contact. Vacuum bellows decouple pipe stiffness.
- **Thermal ramp in couplings:** pre-cooling/pre-heating 5–15 s synchronized with material diffusivities. Contact pressure regulated with Belleville washers or pneumatic pads, keeping Hertz stresses < 50% of yield limit.

(iii) Instantaneous imbalance and active control. Each shot ($E_{\text{fus}} = 20$ MJ) generates local dynamic perturbations (order 0.1–0.5 kN equivalent) associated with asymmetric heat deposition and dome geometry. The invention ensures global balance by:

- **Diametral scheduler:** control inhibits adjacent shots and activates diametral pairs.
- **Passive damping:** TMDs (tuned mass dampers) + eddy current dampers (Cu plates + NdFeB magnets).
- **Active control:** magnetic bearings at hub with MIMO state–space/LQG loops, as in cryogenic gas turbines.

(iv) Vibration and non-uniform shots. Asynchronous or failed shots may excite rotor bending modes ($L = 19$ m). Mitigation includes:

- **Tuned TMDs:** placed on ring, tuned to first bending mode.
- **Redundant bearings:** duplex angular + hybrid magnetic. Cross-seals minimized.
- **Active IMU control:** IMU network on ring + actuators (voice coils) apply MIMO control to reject 1× and subsynchronous harmonics.
- **Mass balancing:** cartridges calibrated ±20 g·cm. Automatic counterweights correct residual imbalance.

Operational and design notes. At 12 rpm ($\omega = 1.257$ rad/s) and $r = 8.5$ m, the peripheral speed is 10.7 m/s. The Ti–6Al–4V ring is sized with effective section $A_{\text{eff}} \geq 0.012$ m^2 (FS$\geq$ 2) to contain centrifugal loads $\sim$ 4 MN ($N = 60$, $m_{\text{cartridge}} = 5$ t). The isothermal strategy maintains $\Delta T_{\text{cell-ring}} < 40$°C at steady state, reducing differential expansion and LCF fatigue. Flatness/clearance control ensures repeatable coupling with the IGBI radiator, avoiding wear during the staged cooling cycle.

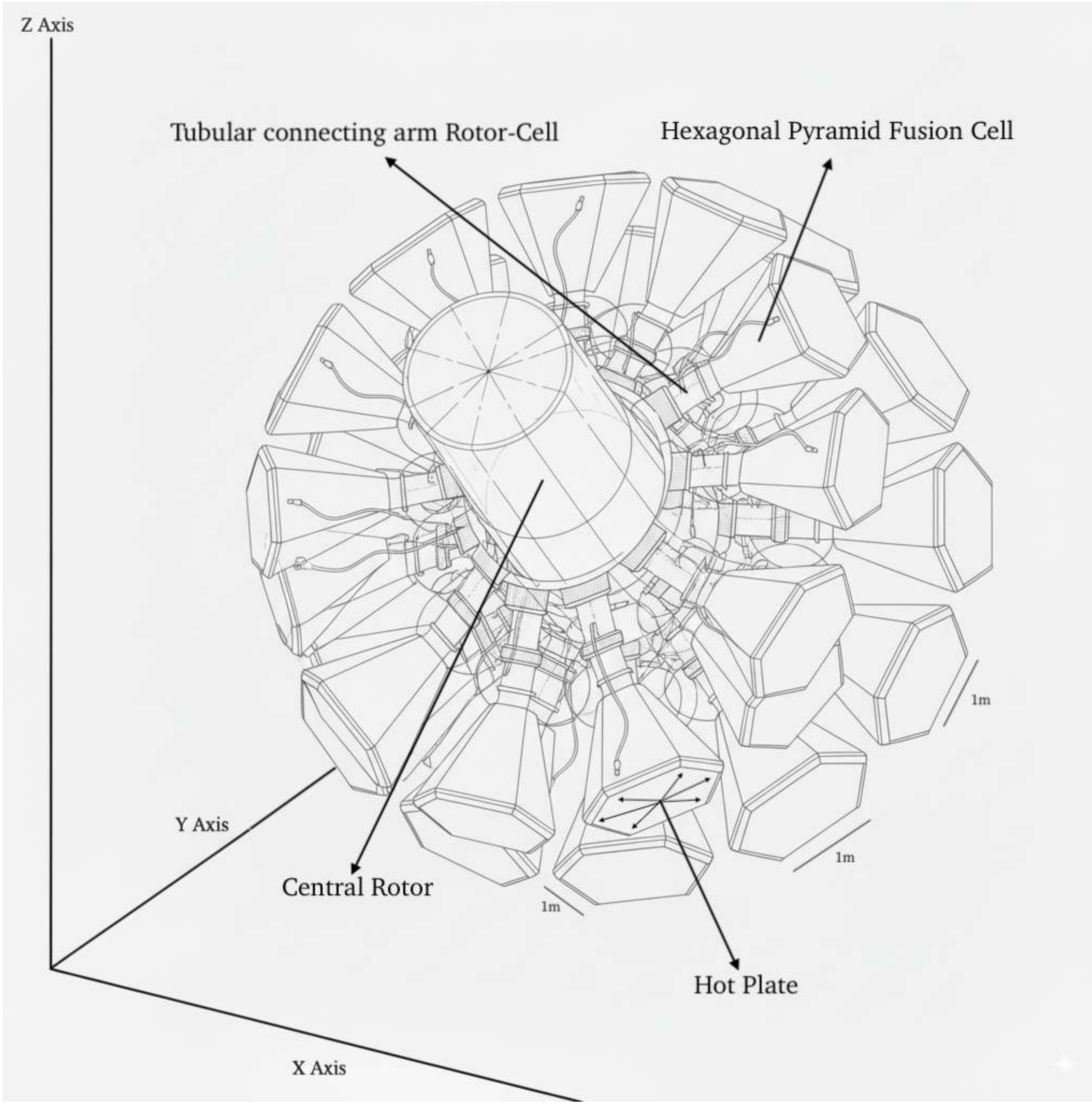

Figure 4: Schematic of a multilayer fusion-cell configuration coupled to the central rotating system.

4.8 Design of the Staged Cooling System

After each ignition, the integrated cartridge (Dome+NEH+Hot–plate) undergoes a thermal spike $T_{\text{peak}} \sim$ 1500–2000 K under fluxes $q \sim 1.0$–1.2 MW/m^2 over $A_{\text{hot}} \sim 2.6$ m^2. To avoid thermal shocks and mechanical wear, a strategy of **staged heat transfer without solid contact** is adopted, comprising three main phases (A–C) and a service window (D).

4.8.1 IGBI interface (pressurized He jets + TZM pin–fins)

- **Principle:** array of pressurized helium micro-jets impinging through a micro-drilled TZM plate, with a TZM *pin–fin forest* (needles) on the radiator face opposite the hot–plate. The controlled gap (0.5–1.5 mm) ensures transfer *without solid contact.*

- **Jet geometry:** holes ⌀0.8–1.2 mm, pitch 5–8 mm (hexagonal pattern), rear plenum chamber; supply pressure 6–10 bar. Typical Reynolds numbers Re $\sim 1.5 \times 10^4$–3×10^4.

- **Pin–fins (TZM):** ⌀1–2 mm, height 8–12 mm, *pitch* 4–6 mm. They increase effective area, disrupt the boundary layer, and homogenize the flow, enhancing local h in the stagnation region.

- **Coefficients and capacity:** $h_{\text{jet}} \sim 6$–12 kW/m^{2}K at stagnation; with $\Delta T_{\text{drive}} \sim 500$–$650$ K, the IGBI *capacity* is $q_{\text{cap}} \sim 3$–7.8 MW/m^2. In operation it is limited by the **wall limit** at $q_{\max} = 1.1$–1.3 MW/m^2.

- **Primary discharge:** with $A_{\text{hot}} = 2.60$ m^2 and $t_{\text{coupling}} = 0.8$–$1.0$ s,

$$E_A \approx q_{\max} A_{\text{hot}} t_{\text{coupling}} \approx 2.3\text{–}3.4 \text{ MJ}.$$

- **He management:** peripheral collectors, particle filtration, purge by–pass and pulsation control to suppress *jet–flapping*; thermal recovery to sCO_2 in the Brayton block.

4.8.2 Sectorized gaseous pre–cooling

- **Stage B1 (He jets):** 4–8 bar, coefficient $h \sim 2$–5 kW/m^{2}K; reduction from 1100 K to 800 K in ∼1.0–1.5 s.

- **Stage B2 (thermal polishing):** combined He/N_2 flow + black radiators ($\varepsilon \sim 0.8$); reduction from 800 K to 600 K in ∼1.5–2.0 s.

4.8.3 Service and maintenance window

- **Duration:** 0.5–1.0 s after cooling.

- **Functions:** inspection (thermography + rapid UT), He purge, flatness metrology, and robotic replacement of NEH sub-cartridges after $\sim 10^5$ shots.

4.8.4 Clearance control and integration

Laser fiducials + CMOS triangulation ensure flatness < 100 μm, lateral error < 150 μm and clearance 0.5–1.5 mm. Piezoelectric micro–stages correct pose in real time. The isothermal ring (Ti–6Al–4V with CO_2 channels) maintains $\Delta T_{\text{cell-ring}} < 40°$C, mitigating differential expansions.

4.8.5 Energy balance per shot

$$E_{\text{base,max}} = q_{\text{allow}}\, A_{\text{hot}}\, t_{\text{coupling}} \;\approx\; 2.6\text{–}5.2\ \text{MJ}.$$

With deposition toward the base $f_{\text{hot}} \approx 0.6$:

$$E_{\text{dep,total}} \approx 4.3\text{–}8.7\ \text{MJ}.$$

The combined efficiency of stages A–C (η_{tot}) is of order 0.65–0.75, sufficient to keep $\Delta T_{\max} < 200$ K per cycle.

Note: the thermal capacity of the IGBI is far above the flux used; operation is **capped by the wall limit** ($q_{\max}$), not by the heat exchanger.

4.8.6 Properties of candidate materials

Fluid	Conductivity k (W/mK)	c_p (J/kgK)	T range (K)
He (8 bar)	0.15	5200	300–1500
NaK	25–30	1000	300–1200
FLiBe	1–2	2400	600–1700
LiPb (17Li–83Pb, advanced option)	12–15	150	500–1600

4.8.7 Margin with respect to structural materials

- **Backplate RAFM/Ti:** $\Delta\sigma < 0.4\,\sigma_y$; gradients $\Delta T < 200$ K/cycle.
- **Rear W–SiC plate:** $k \sim 140$ W/mK; gradients < 50 K/cm, well below cracking threshold.

4.8.8 Scalability

For enlarged hot–plates ($A_{\text{hot}} = 3.5\text{–}4.0\ \text{m}^2$), the cycle is adjusted by increasing t_{coupling} by $\sim 30\%$ and He flow rates by 20%. The staged sequence preserves the same cooling curve, ensuring modular compatibility with rotors of different capacities.

4.8.9 Note on rotary joints

The design avoids **high-temperature liquid-metal rotary joints**: FLiBe circulates in the fixed stator. The cartridge transfers energy only via the IGBI interface or co–rotating pad, simplifying logistics and increasing reliability.

4.9 Architecture of the *Neutron Energy Harvester* (NEH) and material specifications

The multilayer NEH blanket constitutes the primary interface for capture and conversion of fusion energy (14.1 MeV neutrons and 3.5 MeV α particles). Its design optimizes: (i) resistance to repetitive pulsed loading, (ii) neutron moderation/absorption down to the ^{6}Li capture window, (iii) tritium breeding with TBR ≥ 1.05, and (iv) heat extraction at high flux density, integrated in the **cell cartridge** (Dome + *hot-plate* + NEH) described in Sec. 4.1 and Sec. 4.6.

Scope and geometric variants.

- **Wall/blanket** (pyramidal faces): thin stack, distributed load.
- **Base (*hot-plate*) with dome:** reinforced first wall and larger hydraulic section, increasing capture fraction ε_{cap} by geometric flow bias.

4.9.1 Functional stack (plasma face → interior)

1. **PFC (*Plasma-Facing Component*):** W or W–SiC cermet.
   Wall: t=20–30 mm; *Base*: t=40–50 mm. Functions: stop α ($\sim$20% E_{fus}), withstand thermal shock, first n spectral conditioning.
2. **Moderator/multiplier:** Be/BeO and/or C/SiC, t=40–60 mm. Functions: slow down 14 MeV n → 0.1–1 MeV; multiplication $(n, 2n)$ in Be.
3. **Breeder + coolant:** baseline **FLiBe** (Li_2BeF_4) enriched in ^{6}Li, t=60–80 mm, channels ∅20–30 mm. *Option:* LiPb (17Li–83Pb) (see Appendix **??**).
4. **Absorber/fine shield:** B_4C / Gd_2O_3 / Hf, t=20–30 mm.
5. **Rear structural plate:** RAFM or Ti–6Al–4V, $t \simeq 20$ mm, with microchannels and cartridge anchors.

4.9.2 Thermo–mechanical properties (guideline ranges)

Table 6: Properties by layer/material (indicative *in situ* design values).

Material	T [K]	k [W/mK]	c_p [kJ/kgK]	ρ [g/cm^3]	CTE [10^{-6}/K]	Guideline limit
W (PFC)	800–1200	120–170	0.13–0.16	19.3	4.5–5.0	$\Delta T_{\rm pulse} \leq 300$ K; $\sigma_{\rm eq} < 0.6\,\sigma_y$
W–SiC (PFC)	800–1200	60–110	0.20–0.35	11–15	5–6	Toughness ↑, thermal shock ↑
Be / BeO (mod.)	600–900	180–220	1.6–1.9	1.85 / 3.0	11–12	Encapsulated due to toxicity
C/SiC (mod.)	700–1100	120–180	0.75–0.9	2.9–3.2	4–5	Low CTE; good diffusivity
LiPb (breeder)	900–1100	12–16	0.20–0.30	9.4–10.5	25–30	Conductor; MHD option (App. A.1)
FLiBe (breeder)	900–1050	1–2	1.9–2.2	1.9–2.1	20–22	Electrically insulating; chemically stable
B_4C (absor.)	600–900	15–30	0.75–0.85	2.5–2.6	4–5	^{10}B: high thermal σ_a
Gd_2O_3 (absor.)	600–900	6–10	0.35–0.45	7.4	8–9	Gd-157: very high thermal σ_a
Hf (absor.)	600–900	20–23	0.15–0.20	13.3	5–6	Ductile absorber in plates
RAFM (plate)	600–800	15–25	0.45–0.60	7.7–7.9	11–12	Low activation; weldability
Ti–6Al–4V (plate)	500–800	6–7	0.55–0.70	4.43	8–9	$\sigma_y(500^\circ\mathrm{C}) \sim 450$–600 MPa

4.9.3 Neutronic parameters and TBR

- **Initial conditioning** in PFC (W/W–SiC): γ attenuation and controlled sputtering.
- **Moderation/multiplication:** Be/BeO reduces E_n to 0.1–1 MeV (^{6}Li window) and multiplies flux via (n,2n).
- **Breeder:** baseline FLiBe with enriched ^{6}Li sized for TBR ≥ 1.05 at real angular coverage; LiPb option (App. **??**) when volumetric power density is prioritized.
- **Absorber:** B_4C / Gd_2O_3 captures residual thermal tails and protects the rear plate.

4.9.4 Hydraulic and thermal sizing (baseline FLiBe)

Energy closure per cartridge (consistent with Secs. 4.4 and 4.2).

$$Y_{\rm fus} = 20\text{ MJ}, \quad f_{\rm cell} = 0.25\text{ Hz}, \quad \varepsilon_{\rm cap} = 0.90, \quad \xi = 0.90, \quad \eta_{\rm el} = 0.50.$$

Thermal power per cycle per cartridge:

$$P_{\rm th,in} = Y_{\rm fus}\, f_{\rm cell}\,(\varepsilon_{\rm cap}\,\xi) = 20 \times 0.25 \times 0.81 \;\approx\; \mathbf{4.05}\ \mathrm{MW_{th}}.$$

Net electric power (without MHD in the main chain):

$$P_{e,\rm cell} = P_{\rm th,in}\,\eta_{\rm el} \;\approx\; 4.05 \times 0.50 \;\approx\; \mathbf{2.03}\ \mathrm{MW}.$$

Required FLiBe flow. Taking $\Delta T_{\mathrm{FLiBe}} = 150$ K (e.g. $950 \to 1100$ K) and $c_p \simeq 2.0$ kJ/(kg K):

$$\dot{m}_{\mathrm{FLiBe}} = \frac{P_{\mathrm{th,in}}}{c_p\,\Delta T} \approx \frac{4.05\times10^6}{2000\times150} \approx \mathbf{13.5}\ \mathrm{kg/s}.$$

Design guideline: $\dot{m} = 12{-}18$ kg/s per cartridge (valve-adjustable) with typical channel velocities $u = 1{-}3$ m/s.

Channel geometry and velocities. For circular channels ⌀20−30 mm, the total hydraulic area required for $u \sim 2.0$ m/s is:

$$Q = \frac{\dot{m}}{\rho} \approx \frac{13.5}{2000} \approx 6.8\times10^{-3}\ \mathrm{m^3/s}, \quad A_{\mathrm{tot}} = \frac{Q}{u} \approx 3.4\times10^{-3}\ \mathrm{m^2}.$$

With 36 channels of ⌀20 mm (unit area $\approx 3.14\times10^{-4}$ m^2), $A_{\mathrm{tot}} \approx 1.13\times10^{-2}$ m^2 $\Rightarrow u \approx 0.6$ m/s (very conservative regime). It is recommended to modulate the number of channels (24–60) to keep $u \in [1,3]$ m/s and $\mathrm{Re} \sim 10^4{-}10^5$ (turbulent).

Dimensionless numbers (FLiBe, 1000 K).

$$\mathrm{Re} = \frac{\rho u D_h}{\mu}, \quad \mathrm{Pr} = \frac{\mu c_p}{k}\ (\sim 10{-}15), \quad \mathrm{Pe} = \mathrm{Re}\,\mathrm{Pr}.$$

For D_h=25 mm, u=2 m/s, $\mu\approx6\times10^{-3}$ Pa s, $\rho\approx2000$ kg/m^3: $\mathrm{Re} \approx 1.7\times10^4$ (turbulent). With k=1.5 W/mK, $\mathrm{Pr} \approx 8{-}12$. Use turbulent correlations with high Pr and short-entry thermal effects (dome blocks).

LiPb option (quick reference; details in App. ??). With $c_p \sim 0.2$ kJ/(kg K) and $\Delta T \sim 200$ K, the same $P_{\mathrm{th,in}}$ requires $\dot{m}_{\mathrm{LiPb}} \sim 100$ kg/s. Recommended $u = 3{-}5$ m/s, redox control, and ceramic coatings in the channel.

4.9.5 Chemical management and tritium extraction

- **FLiBe (baseline):** redox potential control (Be/BeF_2 pairs), T extraction via He bubbling and cold traps; compatibility with ceramic insulators and metallic C-seals.
- **LiPb (option):** Al/Zr getters, degassing, membrane permeators for T_2/HT; protective coatings (selective aluminization, nitrides) at interfaces.
- **TBR:** ^{6}Li enrichment and full angular dome coverage guarantee TBR ≥ 1.05 at nominal cartridge power.

4.9.6 Fabrication, QA/QC and maintenance

- **Segmented PFC:** W/W–SiC facets (brazing or diffusion), RT/UT on joints.
- **Microchannel blocks:** L-PBF or HIP+machining; internal coating SiC/Al_2O_3.
- **Back plate (RAFM/Ti):** forging+LAM, stress relief; INVAR inserts for CTE grading.
- **In-service NDT:** phased-array UT, eddy currents; DTS fiber optics in channels.
- **Modules:** BEM (Dome+NEH+*hot-plate*) and SC-NEH (lateral sub-cartridge) as per Sec. 4.6.

4.9.7 Limits and lifetime

- PFC thermal shock: $\Delta T_{\rm pulse} \lesssim 300$ K; gradient <5–8 K/mm.
- Equivalent stresses: $\sigma_{\rm eq} < 0.6\,\sigma_y(T)$; Miner $\sum n_i/N_i < 0.2$ per cartridge.
- Neutron fluence: replacement before 10–20 dpa in PFC/moderator (1–3 year window depending on cadence).
- Corrosion/erosion: $u \leq 5$ m/s on walls; redox control + coatings at high-shear corners.

4.9.8 Performance closure (baseline without MHD in chain)

$$
\begin{aligned}
&Y_{\rm fus} = 20\ \text{MJ}, \quad f_{\rm cell} = 0.25\ \text{Hz},\\
&\varepsilon_{\rm cap} = 0.90,\ \xi = 0.90\ \Rightarrow\ P_{\rm th,in} \approx 4.05\ \text{MW}_{\rm th},\\
&\eta_{\rm el} = 0.50\ \Rightarrow\ P_{e,\rm cell} \approx \mathbf{2.03\ MW}.
\end{aligned}
$$

Note: the integration of MHD conversion with LiPb, its *figures of merit* (Ha, N, Rm) and partial electrical gains are documented separately in Appendix A.1 and are not part of the **baseline** energy chain in this section.

4.10 Maintenance and Cartridge Replacement

Preliminary note. The physical architecture of the cartridges (dome+NEH+hot plate) is developed in Sec. 4.6, while their energy role per cell is analyzed in Sec. 4.1.1. Here we address exclusively the logic of maintenance and replacement at the system scale.

Hot-plate cartridge design. Each fusion cell base integrates a modular **NEH cartridge** of 200–300 mm, with typical stratification:

- **Front tile** (20–30 mm): W–SiC, exposed to direct flux, designed to withstand thermal shocks $\Delta T \sim 200$–300 K and 10^5 cycles.
- **Intermediate slab** (150–200 mm): breeder/coolant (FLiBe enriched in ^{6}Li), with channels ⌀20–30 mm for $\dot{m} = 50$–100 kg/s.
- **Back plate** (30–50 mm): RAFM steel, with microchannels for secondary evacuation and shielding.

Mounted on a *three-point kinematic mount*, with radial locking pins and prismatic guides ensuring positional repeatability of ±0.2 mm even after dozens of replacements.

Robotic replacement system. The rotor operates in a *tick-discretized* regime (Sec. 4.3), such that a cell periodically aligns with fixed service stations:

1. **Station N_x (extraction):** a robotic arm releases the pins, disconnects services (fluid, sensors), removes the degraded cartridge, and places it into a shielded container with heavy/borated water for cooling.

2. **Station N_{x+1} (insertion):** a second arm positions a new cartridge, aligns it with laser fiducials, and secures it with automatic pins. Sealing is validated with force sensors and 3D vision.

Cycle time: 45–60 s per cartridge, compatible with continuous operation.

Manipulator candidates. Industrial precedents demonstrate feasibility:

- Fanuc M-2000iA/2300: payload 2.3 t, reach 3.7 m, repeatability ± 0.2 mm.
- KUKA KR QUANTEC ultra: payload 300 kg, repeatability ± 0.06 mm (applicable to optical cartridges).
- AREVA/Westinghouse telemanipulators: designed for fuel rods in fission reactors.
- ITER Remote Handling System: replacement of FW modules of 4–6 t in irradiated environments.

Replacement interval. For loads ~ 1 MW/m^2 and life $N_{\text{cycles}} \sim 10^5$:

$$t_{\text{life}} = \frac{N_{\text{cycles}}}{f_{\text{cell}}} = \frac{10^5}{0.25} \approx 1.1 \times 10^6 \text{ s} \approx 4.6 \text{ days}.$$

A replacement is scheduled every 3–5 days per cartridge. A staggered plan ensures that ∼2–3 cartridges are replaced per day in steady operation, without net power loss.

Continuous operation and passive safety.

- The rotor halts in intervals of 0.67 s, advancing in fixed ticks; each cell, during those 0.67 seconds, is in a different state of the cycle and performs its function within that time frame.
- Degraded cartridges are sealed in borated steel containers for transport/reprocessing.
- Redundant manipulators ensure continuity in the event of failure.
- Global power impact: instantaneous drop $< 2\%$ and full recovery within ∼1 min.

Management of optical consumables and sensors. Windows, filters, and optical cartridges are integrated as interchangeable consumables using the same manipulators. With a lifetime of $\sim 10^4$ shots per window (~ 11 h at 0.25 Hz), replacement is practically daily. The cost will depend on unit price; the development of coatings (Si_3N_4, DLC) is being considered to extend service life to 3–5 days, reducing logistics and operating expense.

Operational balance. The modular replacement system maintains:

$$\eta_{\text{avail}} > 0.98 \quad \text{(global plant availability)},$$

ensuring continuity of electrical output and reducing inventory of critical parts. The strategy turns maintenance into a *programmed and continuous* operation, more akin to replacing printer cartridges than to major outage cycles of a conventional reactor.

4.11 Laser and Sensor Assembly (Apex + Edge Pods)

Port placement strategy. To minimize neutron flux and direct thermal load, no ports are placed on the base or at its vertices. The final architecture combines:

- **Apex port (primary coaxial beam):** traverses the symmetry axis of the truncated hexagonal pyramid, delivering the main beam to the target through internal folding optics.
- **Edge pods (auxiliary oblique beams):** three or four pods embedded in the upper edges of the pyramid, at $\sim 2/3$ height relative to the base, each with an obliquity of 15–25° toward the target.

Laser cluster and redundancy. Each port mounts a *triple cluster* of high-energy lasers, operating in round–robin mode to distribute fluence, with hot–standby redundancy in case of failure.

- **Tripled Nd:glass (351 nm):** NIF/LMJ reference; pulse energy 0.3–0.7 MJ.
- **KrF excimer (248 nm):** high repetition, applicable to auxiliary pods.
- **OPCPA petawatt:** ultrashort startup/conditioning pulses.

The energy delivered per port is 0.3–0.7 MJ; with 4–5 active ports the total energy on target is 1–2 MJ. Deformable mirrors maintain phase error < 10 ps and overlap < 0.5 mm on the pellet.

Optical protection and consumables. Each port incorporates:

- **Sacrificial windows:** baseline lifetime 10^4 shots.
- **Segmented faceted windows (8–16 sectors):** increase effective lifetime by $\times$8–12, reducing OPEX from ~ 70 M€/year (unmitigated) to ~ 1 M€/year for a 24-cell FRE rotor.
- **Faceted ceramic shutters:** closing ≤ 2 ms during the harvest phase, distributing erosion.
- **Local dry He purges:** prevent condensate deposition and extend optical lifetime.

Replacements are performed hot using the same robotic manipulators as for the cartridges (Sec. 4.10), homogenizing maintenance logistics.

Integrated sensorics.

- **Coaxial interferometry:** through the axial port, measuring implosion and symmetry.
- **Fast photodiodes and scintillators:** in edge pods, behind Be/SiC shielding, for timing and neutron spectrum.
- **Fiber-optic telemetry:** data + clock distributed to the central bus; closed-loop pointing correction (< 1 mrad).

- Without segmentation: cost >70 M€/year in optical consumables (windows, filters) for a 24-cell FRE.
- With coatings + segmentation ($\times 10^5$ effective shots/window): cost $\sim$ 7–14 M€/year.
- With **12-sector segmented window** + He purge: cost $\sim$ 0.6–1.2 M€/year, level compatible with reference OPEX.

This architecture makes maintenance economically viable, eliminating optics as a bottleneck.

Parameter	**Nominal**	**Range**
No. of ports	1 apex + 3 pods	1 apex + 4 pods
Incidence (pods)	20°	15–25°
Energy/port	0.5 MJ	0.3–0.7 MJ
Total target energy	1.5 MJ	1–2 MJ
Temporal phase error	< 10 ps	< 20 ps
Pellet overlap	< 0.5 mm	< 1.0 mm
Window lifetime (unmitigated)	10^4 shots	5×10^3–2×10^4
Effective lifetime (segmented)	1.0–1.2 $\times 10^6$	depends on m sectors
FRE windows OPEX (24 cells)	0.6–1.2M€/year	(with mitigation)
Shutter time	≤ 2 ms	≤ 5 ms

Table 7: Optical and sensor parameters (apex port + edge pods).

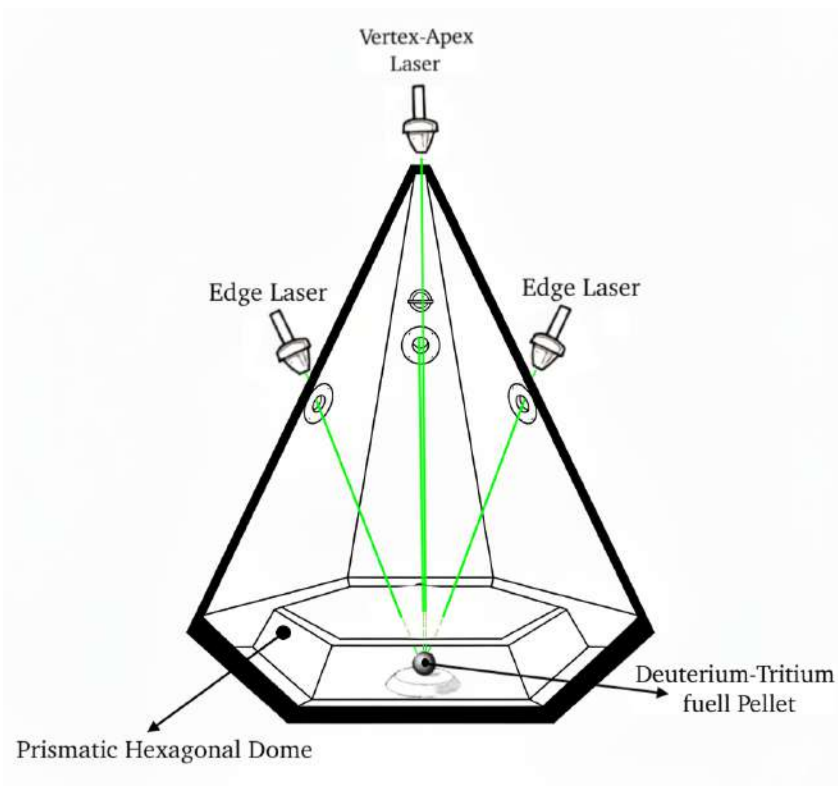

Figure 5: Schematic cross-section of a fusion cell (truncated hexagonal pyramid with NEH dome). The **coaxial beam** from the apex and the **auxiliary oblique beams** from edge pods are represented. All converge on the **D–T pellet**, distributing energy and reducing localized damage on a single port.

4.12 Unit Cost and Mass per Cell (bottom–up model, RAFM structure + W–SiC PFC + FLiBe)

Objective and scope. Bottom–up estimation of **unit cost** and **mass** for a **hexagonal pyramidal cell** in nominal configuration: **RAFM steel structure** (low activation), **W–SiC PFC** on *hot–plate* with dome, **FLiBe breeder** enriched in ^{6}Li, and **RAFM back plate**. This configuration materializes the *minimum-cost MVP*, while maintaining adequate thermal and mechanical performance.

Key processes (RAFM structure).

- **Lamination + CNC machining:** RAFM panels 12–25 mm; drilling/manifolds; flange surfacing.
- **EBW/GTAW welding in inert chamber:** panel joints, ribs, and supports; controlled preheating.
- **Modular assembly:** ribs and stiffeners, docking flanges, cartridge seats, and positioning keys.
- **QA/QC:** phased-array UT, eddy current testing, and leak testing (He $< 10^{-9}$ mbar·L/s) in feedthroughs and flanges.

Geometric assumptions (NEH with dome). Consistent with Secs. 4.9 and 4.8: hot base area $A_{\text{hot}} \approx 2.6$ m^2; W–SiC PFC $t_{\text{PFC}} = 45$ mm; **FLiBe breeder** $t_{\text{br}} = 120$ mm (base with dome); **RAFM back plate** $t_{\text{back}} = 30$ mm; external pyramidal structure in RAFM (12–20 mm panels + ribs).

Masses (nominal). Densities: $\rho_{\text{WSiC}} \approx 12{,}500$ kg/m^3, $\rho_{\text{FLiBe}} \approx 2{,}000$ kg/m^3, $\rho_{\text{RAFM}} \approx 7{,}800$ kg/m^3.

$$\begin{aligned}
m_{\text{PFC}} &= A_{\text{hot}}\, t_{\text{PFC}}\, \rho_{\text{WSiC}} = 2.6 \times 0.045 \times 12{,}500 \;\approx\; \mathbf{1{,}463}\ \text{kg},\\
m_{\text{br}} &= A_{\text{hot}}\, t_{\text{br}}\, \rho_{\text{FLiBe}} = 2.6 \times 0.12 \times 2{,}000 \;\approx\; \mathbf{624}\ \text{kg},\\
m_{\text{back}} &= A_{\text{hot}}\, t_{\text{back}}\, \rho_{\text{RAFM}} = 2.6 \times 0.03 \times 7{,}800 \;\approx\; \mathbf{608}\ \text{kg},\\
m_{\text{struct}} &\approx \text{RAFM (walls+ribs)} \;\Rightarrow\; \mathbf{3.0\text{–}3.6}\ \text{t}.
\end{aligned}$$

Note: The higher Young's modulus of RAFM (∼200 GPa) allows slightly thinner panels than Ti while maintaining flexural stiffness; the lower thermal conductivity of Ti compared to RAFM (6–7 vs 15–25 W/mK) makes RAFM preferable for lateral thermal spreading of the base.

Raw material costs (bulk procurement). Guide prices: RAFM ∼ 7 EUR/kg, effective W–SiC ∼ 110 EUR/kg, FLiBe enriched (base with dome) *equivalent cost* ∼0.30–0.60 M EUR/cell (includes ^{6}Li surcharge and nuclear-grade fuel salt).

$$\begin{aligned}
C_{\text{mat}}(\text{RAFM struct}) &\approx (3.3\ \text{t}) \times 7 \;\approx\; \mathbf{0.023}\ \text{M EUR},\\
C_{\text{mat}}(\text{WSiC PFC}) &\approx 1.463\ \text{t} \times 110 \;\approx\; \mathbf{0.161}\ \text{M EUR},\\
C_{\text{mat}}(\text{FLiBe}) &\approx \text{nominal } \mathbf{0.45}\ \text{M EUR}\ \ (0.30\text{–}0.60),\\
C_{\text{mat}}(\text{RAFM back}) &\approx 0.608\ \text{t} \times 7 \;\approx\; \mathbf{0.004}\ \text{M EUR}.
\end{aligned}$$

Process and QA costs (order of magnitude).

- **RAFM structure (lamination+machining+welding+QA): 0.20–0.26** M EUR (nominal **0.22**).
- **NEH cartridge (W–SiC PFC machining, assembly, FLiBe cleaning/loading, microchannels, NDT): 0.35–0.50** M EUR (nominal **0.42**).

Laser drivers, sensors, and auxiliaries (series).

- **Lasers + optics/fiber + windows/shutters + sensors: 0.80–1.00** M EUR (nominal **0.90**).
- **Auxiliaries (piping/manifolds/valves/supports/insulation): 0.20–0.35** M EUR (nominal **0.28**).

Block	**Nominal mass**	**Nominal cost (M EUR/cell)**
RAFM structure (lamination+mach.+weld.)	3.0–3.6 t	Mat. ∼0.023; Proc. ∼0.22 ⇒ **0.24**
W–SiC PFC (45 mm)	1.46 t	**0.161**
FLiBe breeder (120 mm)	0.62 t	**0.45**
RAFM back plate (30 mm)	0.61 t	**0.004**
NEH: materials (subtotal)	∼2.69 t	**0.615**
NEH: processes & QA	–	**0.42**
Lasers + sensors	≪ 0.1 t	**0.90**
Auxiliaries (fluid/supports)	0.2–0.3 t	**0.28**
Totals per cell	∼ **6.4–7.0** t	**2.50 M EUR**

Table 8: Bottom–up breakdown of mass and cost per cell with RAFM structure and backplate, W–SiC PFC, and FLiBe breeder (baseline MVP). Typical ranges: 2.35–2.95 M EUR/cell depending on supplier and volume.

Summary (MVP) and reinforcement options

Cell (MVP): $m_{\text{cell}} \approx 6.7$ t; $C_{\text{cell}} \approx \mathbf{2.50}$ M EUR (range 2.35–2.95).
Optional structural reinforcement: if verification of centrifugal/shock loads indicates low margins, add *compression rings* at the base edge, radial *stays*, and longitudinal *stringers* in RAFM. Typical impact: +0.2–0.5 t and +0.05–0.12 M EUR per cell, maintaining compatibility with *docking* and IGBI.

Material sensitivity (per cell):
• *Solid W* instead of W–SiC: +0.15–0.30 M EUR, +0.7–0.9 t. • *LiPb* instead of FLiBe: $m_{\text{br}} \to 4.7$ t; C_{mat} similar or lower, but +4 t of total mass (penalizes inertia).
• *Ti structure* (SPF/DB+WAAM) instead of RAFM: −1.5–2.0 t, but +0.25–0.45 M EUR/cell (processes and raw material).

Technical notes. (1) **RAFM baseline** reduces CAPEX compared to Ti and improves lateral thermal spread relative to a Ti backplate. (2) **FLiBe baseline** minimizes the mass of *fuel salt* in the dome base; the ^{6}Li enrichment surcharge is included in the range. (3) **Structural reinforcements** (rings, stays, stringers) are modeled as add-on *kits* per cell based on rotor dynamics and thermal shock results, without altering interfaces with service stations or IGBI.

4.13 Cost per rotor and per campus

Assumptions.

- Baseline cost per cell (RAFM + W–SiC + FLiBe): **2.50** M€.
- Optional structural reinforcement (rings, stays, stringers): +0.05–0.12 M€/cell (nominal +0.08).
- Net power per cell (calibration Secs. 4.1–4.3): $P_{e,\text{cell}} = 2.03$ MW.

Cost per rotor (N cells).

$$C_{\text{rotor}}^{\text{base}}(N) = 2.50\,N \quad [\text{M€}], \qquad \Delta C_{\text{ref}}(N) = (0.05\text{–}0.12)\,N \quad [\text{M€}].$$

Configuration	N	$C_{\text{rotor}}^{\text{base}}$ [M€]	$C_{\text{rotor}}^{\text{nom+ref}}$ [M€]	$C_{\text{rotor}}^{\text{range+ref}}$ [M€]
MVP	18	45.0	**46.44**	45.9 – 47.16
FRE (reference)	24	60.0	**61.92**	61.2 – 62.88
High capacity	60	150.0	**154.80**	153.0 – 157.2

Table 9: Rotor cost with baseline 2.50 M€/cell and optional reinforcement (nominal +0.08 M€/cell).

Specific capital (cell hardware only).

$$\frac{C_{\text{rotor}}^{\text{base}}}{P_{\text{rotor}}} = \frac{2.50\,N}{2.03\,N} \approx \mathbf{1.23}\ \text{M EUR/MW}_{\text{el}}, \quad \frac{C_{\text{rotor}}^{\text{nom+ref}}}{P_{\text{rotor}}} \approx \mathbf{1.27}\ \text{M EUR/MW}_{\text{el}}.$$

($P_{\text{rotor}} = 2.03\,N$ MW; reinforcement barely alters the per-MW ratio.)

Campus cost (48 rotors).

- **Campus with FRE rotors (24 cells):**

  $$C_{\text{campus}}^{\text{base}} = 48 \times 60.0 = \mathbf{2{,}880}\ \text{M€}, \quad C_{\text{campus}}^{\text{nom+ref}} = 48 \times 61.92 = \mathbf{2{,}972.16}\ \text{M€}.$$

  Range with reinforcement: $48 \times [61.2,\ 62.88] = [2{,}937.6,\ 3{,}018.24]$ M€.

- **Campus with 60-cell rotors:**

  $$C_{\text{campus}}^{\text{base}} = 48 \times 150.0 = \mathbf{7{,}200}\ \text{M€}, \quad C_{\text{campus}}^{\text{nom+ref}} = 48 \times 154.8 = \mathbf{7{,}430.4}\ \text{M€}.$$

  Range with reinforcement: $48 \times [153.0,\ 157.2] = [7{,}344,\ 7{,}545.6]$ M€.

Quick Summary

Per cell (baseline): 2.50 M€. **Optional reinforcement:** +0.05–0.12 M€/cell (nom. +0.08).
FRE rotor (24 cells): 60.0 M€ (base) → 61.92 M€ (nom. with reinforcement).
Campus (48 FRE rotors): 2.88 B€ (base) → 2.97 B€ (nom. with reinforcement).
Specific CapEx (cells only): ∼1.23 M€/MW_{el} (base) → ∼1.27 M€/MW_{el} (with reinforcement).
Note: These figures **do not** include power island (Brayton/sCO_2), balance of plant, civil works, cryogenics, vacuum, robotic network/stations, or contingencies; these are added in Sec. 5.

5 Economic Feasibility Study

5.1 Methodology and assumptions

The levelized cost of electricity (LCOE) is calculated as:

$$\mathrm{LCOE} = \frac{\text{CapEx annualized} + \text{OpEx}}{E_{\text{year}}},$$

$$\text{CapEx annualized} = \text{CapEx}_{\text{tot}} \times \mathrm{CRF}(r, n),$$

$$\mathrm{CRF}(r, n) = \frac{r(1+r)^n}{(1+r)^n - 1}.$$

Baseline assumptions.

- Economic horizon $n = 30$ years; discount rate $r = 7\% \Rightarrow \mathrm{CRF} \approx 0.0806$.
- Net power per cell: $P_{e,\text{cell}} = 2.03$ MW.
- Annual production per rotor (example $N = 24$):

$$E_{\text{year}}^{\text{rotor}} = (2.03 \times N) \times 8{,}760 \text{ h}.$$

- Baseline cost per cell (RAFM + W–SiC + FLiBe, with scale): $C_{\text{cell}} = 2.50$ M€.
- Balance of plant (BOP), civil works, integration, cryo, substation, robotics, contingencies:

$$+10\% \text{ (aggressive)}, \quad +15\% \text{ (central)}, \quad +25\% \text{ (high)}, \quad +35\% \text{ (conservative)}.$$

- Annual OpEx (O&M + staff + consumables + licenses): 4% / 5% / 6% of $\text{CapEx}_{\text{tot}}$.
- Average electricity price: $\pi = 75$ €/MWh.

5.2 CapEx per rotor and LCOE (example: 24-cell rotor)

For an FRE rotor with $N = 24$ cells:

$$C_{\text{rotor}}^{\text{base}} = 24 \times 2.50 = 60.0 \text{ M€}, \quad P_{e,\text{rotor}} = 24 \times 2.03 = 48.7 \text{ MW}.$$

Annual production:

$$E_{\text{year}}^{\text{rotor}} \approx 48.7 \times 8{,}760 = 426{,}300 \text{ MWh/year}.$$

All–in CapEx with BOP.

$$\begin{aligned} \text{Aggressive:} &\ +10\% \Rightarrow 66.0 \text{ M€}, \\ \text{Central:} &\ +15\% \Rightarrow 69.0 \text{ M€}, \\ \text{High:} &\ +25\% \Rightarrow 75.0 \text{ M€}, \\ \text{Conservative:} &\ +35\% \Rightarrow 81.0 \text{ M€}. \end{aligned}$$

Annualized CapEx = CapEx $\times$ 0.0806; OpEx = $\alpha \times$ CapEx.

Scenario	All–in CapEx (M€)	Annual CapEx (M€/y)	OpEx (M€/y)	**LCOE (€/MWh)**
Aggressive	66.0	5.32	2.64	$\frac{7.96}{426{,}300} \approx \mathbf{18.7}$
Central	**69.0**	**5.56**	**3.45**	$\frac{9.01}{426{,}300} \approx \mathbf{21.1}$
High	75.0	6.05	4.50	$\frac{10.55}{426{,}300} \approx \mathbf{24.7}$
Conservative	81.0	6.53	4.86	$\frac{11.39}{426{,}300} \approx \mathbf{26.7}$

Table 10: LCOE per FRE rotor (24 cells) with all–in CapEx and proportional OpEx.

5.3 Margins at $\pi = 75$ €/MWh

Revenues per rotor:

$$R^{\text{rotor}} = 426{,}300 \times 75 \approx 31.97 \text{ M€/year}.$$

Scenario	Annual cost (M€/y)	Margin/rotor (M€/y)	Campus margin (48) (M€/y)
Aggressive	7.96	+24.0	+1,150
Central	**9.01**	**+23.0**	**+1,105**
High	10.55	+21.4	+1,027
Conservative	11.39	+20.6	+990

Table 11: Margins at 75 €/MWh. Annual cost = Annualized CapEx + OpEx. Campus: 48 rotors.

Simple payback. For the central case: $\text{CapEx}_{\text{campus}} = 48 \times 69 = 3.31$ B€.

Campus EBITDA $= 48 \times (31.97 - 3.45) \approx 1.37$ B€/year.

$$\text{Simple payback} \approx \frac{3.31}{1.37} \approx \mathbf{2.4} \text{ years}.$$

5.4 Modular deployment and ramp–up

A campus can enter service starting with the first rotor. With *1 rotor every 2 months* (8 years to reach 48) and $\pi = 75$ €/MWh, revenues scale as:

$$R^{\text{year}} \approx N_{\text{rot}} \times 426{,}300 \times 75/10^6 \quad \text{(M€/year)}.$$

Examples: Year 1: $N_{\text{rot}} = 6 \Rightarrow R \approx 192$ M€/year. Year 4: $N_{\text{rot}} = 24 \Rightarrow R \approx 768$ M€/year.
Year 8: $N_{\text{rot}} = 48 \Rightarrow R \approx 1,536$ M€/year.

5.5 Executive summary

- **LCOE (30 y, 7%):** 19–27 €/MWh (central: **21 €/MWh**).
- **Margins at 75 €/MWh:** campus (48 rotors) **+1.1 B€/year**.
- **Simple payback (central):** $\sim$ **2.4 years**.
- **Modular advantage:** revenues from the first rotor, progressive ramp-up, reduced capital risk.
- **Improvement path:** RAFM, WAAM/SPF-DB, barrier coatings, and industrial scale ⇒ further reduction in LCOE and OpEx.

5.6 Impact of material and process improvements

- **RAFM back-plate:** conductivity 15–25 W/mK vs. 6–7 W/mK for Ti–6Al–4V, reducing gradients and improving Brayton efficiency by +0.5–1.5 pp.
- **W–SiC front tile:** neutron resistance and good thermal shock behavior, extending lifetime.
- **SPF–DB and WAAM:** enable complex geometries with 40–60% lower machining cost.
- **Economies of scale:** industrial series $\geq 10^3$ cells reduce CapEx by an additional 5–15%.

These improvements validate the adopted cell cost ($\sim$ 2.50 M€) and consolidate competitive LCOE.

5.7 Consolidated economic comparison (MRFEP vs. fission)

	Rotor 18	**Rotor 24**	**Rotor 32**	**Rotor 60**	**Ref. fission**
Net power (MW)	36.5	48.7	65.0	121.8	$\sim$ 1,200
Annual energy (GWh/y)	320	426	570	1,067	$\sim$ 10,512
Rotor CapEx (M€)	45.0	60.0	80.0	150.0	(variable)
Annual CapEx (M€/y)	3.63	4.85	6.46	12.1	–
OpEx (M€/y)	2.25	3.00	4.00	7.50	–
Annual cost (M€/y)	**5.88**	**7.85**	**10.46**	**19.6**	–
LCOE (€/MWh)	18.4	18.4	18.4	18.3	60–80
Revenues (M€/y, 75 €/MWh)	24.0	32.0	42.8	80.0	$\sim$ 788
Margin (M€/y)	**+18.1**	**+24.2**	**+32.3**	**+60.4**	n/d
Simple payback (years)	2.5	2.5	2.5	2.5	n/d

Table 12: Economic comparison of the MRFEP (18–60 cells per rotor) against a reference fission plant (1.2 GW, 10.5 TWh/year). Assumptions: π = 75 €/MWh, CRF(30y,7%)=0.0806, and OpEx=5% CapEx.

Quick reading.

- 18–60 cell modules provide highly competitive LCOE (18 €/MWh), well below fission (60–80 €/MWh).
- Simple payback around 2.5 years in all cases.
- Modularity allows scaling from MVP (18 cells) to high capacity (60 cells) without losing competitiveness.
- Compared to monolithic fission investment, MRFEP architecture reduces financial risk and accelerates returns.

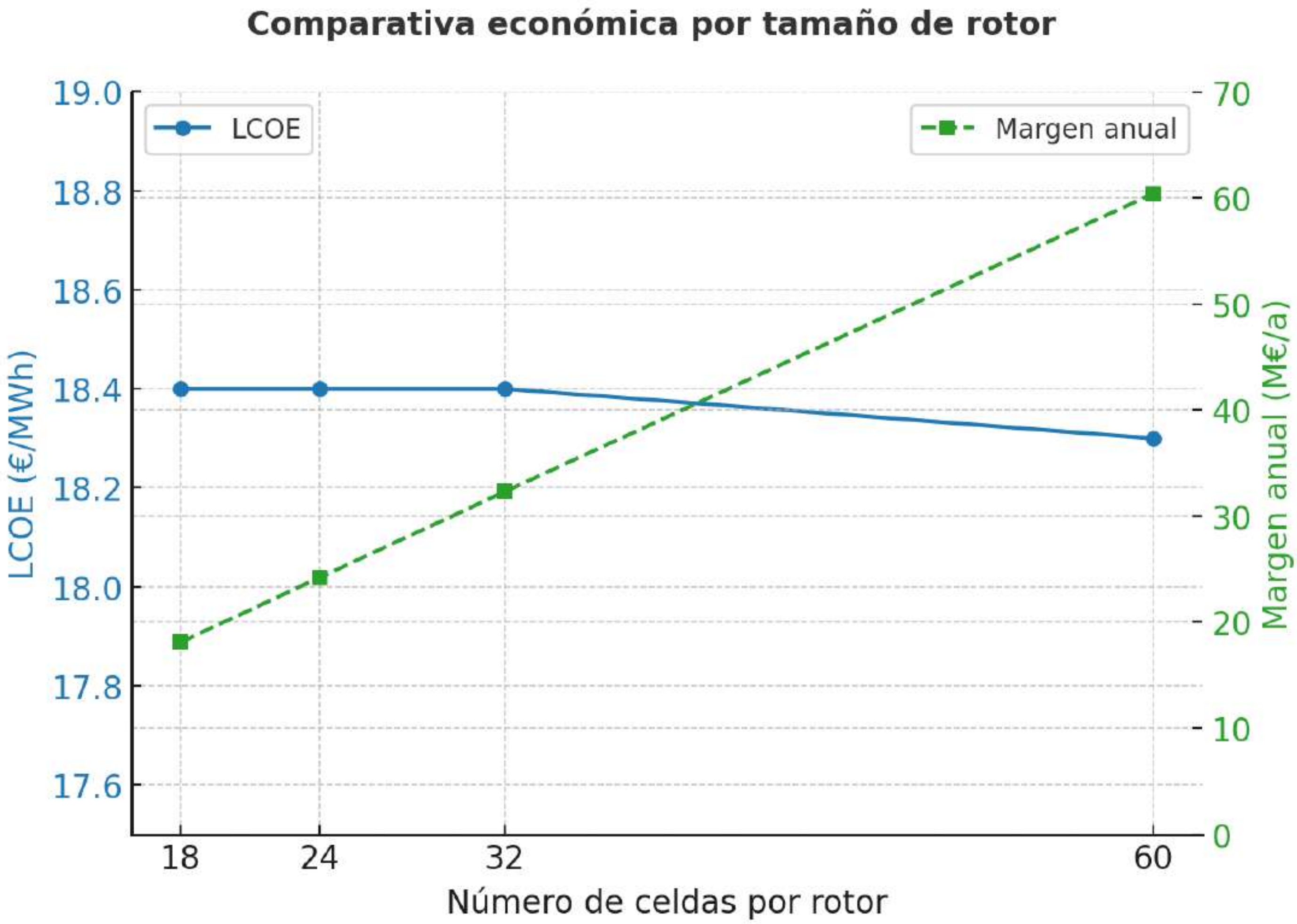

Figure 6: LCOE per rotor as a function of the number of cells.

Figure 7: Impact of rotor size (number of active cells) on the **Levelized Cost of Electricity (LCOE)** and the **annual margin**. The LCOE remains within the competitive range of 18–23 €/MWh, with a decreasing trend as N increases, while the margin scales almost linearly with the number of cells, surpassing 70 M€/year for 60-cell rotors.

6 Real comparison: Fission nuclear plant vs. MRFEP plant

Contrast between an MRFEP campus and a fission plant (PWR/BWR) at real scale. **Baseline** adopted (Secs. 4.1, 4.9, 4.8):

$$P_{e,\text{celda}} = 2.03 \text{ MW}, \quad N_c = 60 \;\Rightarrow\; P_{e,\text{rotor}} = 121.8 \text{ MW}, \quad \eta_{\text{avail}} = 0.95.$$

Annual energy per rotor:

$$E_{\text{year}}^{\text{rotor}} = 121.8 \times 8{,}760 \times 0.95 \simeq \mathbf{1{,}013.6} \text{ GWh/year}.$$

Preliminary notes on fission.

- **Timelines**: 8–12 years until commercial operation (construction, licensing, integrated tests).
- **Footprint**: 70–100 ha with exclusion zones and radiological servitudes.
- **Insurance and liability**: high annual premiums, specific legal frameworks.
- **Waste**: multi-decadal management of spent fuel and decommissioning.

MRFEP footprint rule: **48 rotors** $\approx$ **25 ha** (0.52 ha/rotor).
Capacity: **5.846 GW**; Annual energy: **48.65** TWh/year $\eta_{\text{avail}} = 0.95$).

6.1 Reference case: Almaraz Nuclear Power Plant (Spain)

Almaraz I (1981) and II (1983), two PWRs with installed powers of $\sim 1{,}049$ and $\sim 1{,}044$ MW (total ~ 2.09 GW_{el}); waste, insurance and specific tax burdens apply.[1]

6.2 Scenario A: *Energy equivalence* with a 1.2 GW nuclear plant

Reference fission plant: $P_{\text{nuc}} \approx 1{,}200$ MW.

$$E_{\text{nuc}} = 1{,}200 \times 8{,}760 \approx 10{,}512 \text{ GWh/year}.$$

With $E_{\text{year}}^{\text{rotor}} \approx 1{,}013.6$ GWh/year:

$$N_{r,A} = \frac{10{,}512}{1{,}013.6} \approx 10.37 \;\Rightarrow\; \boxed{\textbf{11 rotors}}.$$

Results:

- **Capacity**: $11 \times 121.8 = \mathbf{1{,}339.8}$ **MW**.
- **Annual energy**: $11 \times 1{,}013.6 \simeq \mathbf{11{,}149.8}$ GWh/year.
- **Footprint**: $11 \times 0.52 \approx$ **5.7 ha**.
- **Revenues at** 75.9 **€/MWh**: $11{,}149.8 \times 10^3 \times 75.9 \simeq \mathbf{0.846}$ B€/year.

Note: with nuclear CF 85–92%, equivalence is reached with 10–11 rotors.

[1] Technical data and public regulations: CSN/MITECO; Law 12/2011 on nuclear civil liability; national waste management plans.

6.3 Scenario B: *Equivalence in land use* (100 ha footprint)

If 48 rotors ⇒ 25 ha, then 100 ha allow for **192** rotors:

$$P_{192} = 192 \times 121.8 = \mathbf{23.386\ GW}, \qquad E_{192} = 192 \times 1{,}013.6 = \mathbf{194.62}\ \text{TWh/year}.$$

Revenues at 75.9 €/MWh:

$$I_{192} \approx 194.62 \times 10^6 \times 75.9 \approx \mathbf{14.77}\ \text{B€/year}.$$

6.4 Direct comparison

Parameter	**Ref. fission (1.2 GW)**	**MRFEP A (11 rotors)**	**MRFEP B (192 rotors)**
Net capacity (MW)	∼ 1,200	1,339.8	23,385.6
Annual production (GWh)	10,512 (100% CF)	11,149.8	194,615
Estimated footprint (ha)	70–100	∼ 5.7	∼ 100
Commissioning	8–12 years	12–18 months (first rotor)	*progressive ramp-up*
Revenues at 75.9 €/MWh	–	∼ 0.846 B€/year	∼ 14.77 B€/year
High-level waste	Yes	No	No

Table 13: Comparison between a reference fission plant and MRFEP scenarios: A (energy equivalence) and B (land equivalence).

Discussion.

- With **11 MRFEP rotors**, annual energy matches (and exceeds) that of a 1.2 GW nuclear plant, occupying only ∼6 ha, with monetization starting from the first rotor.
- With **equal footprint** (100 ha), the MRFEP campus scales to ∼23.4 GW and ∼195 TWh/year, without high-level spent fuel.
- The **granularity** (by rotor/cell) reduces financial and technical risk compared to monolithic projects with ≥8 years *time-to-revenue*.

6.5 Sensitivity notes

- **Electricity price**: at 70−80 €/MWh revenues vary by ±6.5% approx. (linear with energy).
- **Availability**: ±1 pp in η_{avail} ⇒ ±10.14 GWh/year per rotor and ±0.77 M€/year in revenues at 75.9 €/MWh.
- **Thermal efficiency**: +10–20 K on the hot side (RAFM) contribute ∼ 0.5−1.5 pp to Brayton (Sec. 5).

A Complementary and optional technologies

This appendix compiles advanced technologies which, while not part of the reference design (baseline RAFM + W–SiC + FLiBe + Brayton cycle), may be considered as future optimization and extension pathways for the modular MRFEP system.

A.1 Magnetohydrodynamic (MHD) conversion

The use of a conductive liquid breeder (e.g. LiPb) opens the possibility of extracting additional power via direct MHD conversion in integrated ducts. This scheme exploits the Lorentz force on free charges in a flow transverse to a strong magnetic field ($B = 5$–10 T) generated by superconducting coils in the rotor hub.

Physical model.

$$\boldsymbol{j} = \sigma(\boldsymbol{E} + \boldsymbol{v} \times \boldsymbol{B}), \qquad \mathcal{E}_{\text{ind}} = vB\,a,$$

where σ is the conductivity of LiPb, v the flow velocity, and a the electrode spacing. The extractable power density is:

$$p = \sigma B^2 v^2 \frac{K}{(1+K)^2}, \quad p_{\max} = \tfrac{1}{4}\sigma B^2 v^2 \ \ (K = 1).$$

Design example.

- Rectangular duct: $a = 30$ mm, $h = 150$ mm, $L = 1.0$ m.
- Flow: $v = 3$ m/s, $\sigma = 10^6$ S/m, $B = 5$ T.
- Net power: ~0.14 MW/duct (with efficiency $\eta_{\text{elec}} \sim 0.6$).

Scaling. With two ducts per cartridge and 60 cartridges per rotor:

$$P_{\text{MHD,rotor}} \approx 15\text{–}18 \text{ MW},$$

providing 10–15% additional output, with ohmic heat returned to the Brayton cycle. The technology presents material challenges (electrodes, corrosion) and is considered **optional, not included in the baseline economics**.

A.2 Direct conversion of radiation and particles

Another exploratory pathway is direct capture of energy from charged particles and high-energy radiation:

- **Electrostatics for alphas:** high-voltage grids to convert α kinetic energy into electricity.
- **Thermionic/photovoltaic cells**: partial conversion of thermal radiation and bremsstrahlung.
- **Gamma radiation capture**: still at a very preliminary stage, with low yields.

These options are of academic interest but are not included in the baseline energy balance.

A.3 Advanced materials and hybrid breeders

Alternative configurations to the FLiBe baseline can be considered:

- **Liquid LiPb**: high performance for tritium breeding, but penalization in mass and higher corrosivity.
- **Be/SiC**: as a neutron multiplier, compatible with RAFM.
- **MHD-compatible coatings**: TiN, SiC, Al_2O_3 to reduce parasitic currents in conductive flows.

These options are classified as exploratory and for selective application.

A.4 Other future optimization routes

- **HTS superconductors**: more compact field coils with reduced cryogenic demand.
- **Integrated power electronics**: MPPT and DC/AC conversion in each cartridge, for greater flexibility of grid coupling.
- **High-repetition optics**: deformable mirrors and ultrafast OPCPA for operation in regimes >0.5 Hz.

Taken together, these complementary technologies represent possible **evolutionary extensions** of the MRFEP. The present study focuses on the baseline architecture validated in cost and performance, leaving these pathways as a field for future research and development.

B Example of a Full-Scale MRFEP Plant Implementation

This section describes a reference full-scale plant design for a *Modular Rotary Fusion Energy Plant* (MRFEP) based on a single rotor stack with $N = 60$ hexagonal pyramidal cells arranged in three axial tiers (20 cells per tier). The values presented are of *order of magnitude*, indicative and subject to civil/MEP refinement, and serve as a framework for comparison with fission plants in Sec. 6.

B.1 Site layout and land requirements

General plot. A plant with $P_{\text{el,net}} \simeq 26$–50 MW (Brayton+MHD) can be deployed on a fenced plot of ∼1–1.5 ha (12,000–15,000 m^2), including main buildings, service yards, air-coolers or dry coolers, and a compact substation (132–220 kV). The footprint of the main power block is ∼0.3–0.5 ha.

Zoning. The site is divided into:

1. **Reactor Building (RB)**: houses the rotor stack and biological shielding.
2. **Power Conversion Building (PCB)**: Brayton sCO_2 turbomachinery, heat exchangers and MHD converters.
3. **Auxiliaries**: vacuum, cryogenics, tritium handling, water treatment.
4. **Administration and Control Building (A&C)**: control room, offices, QA/QC, HSE.
5. **Electrical substation**: grid connection, transformers and MCC.

B.2 Reactor Building (RB): geometry and shielding

Stack envelope. Each tier houses 20 cells with inner diameter $D_{\text{floor}} \approx 19$–20 m and clear height $H_{\text{floor}} \approx 6$ m (ignition, coupling, cooling, inspection bay). The complete three-tier stack requires $H_{\text{stack}} \approx 18$ m.

Biological shielding. The RB integrates an inner lining of Ti-6Al-4V (50–80 mm), structural steel ribs, and a heavy concrete wall (barite/steel) of $T_{\text{bio}} \approx 1.5$–2.0 m. The radius develops from the center: $R_{\text{cells}} \sim 9.5$ m, service ring (1–1.5 m) and shielding (1.5–2.0 m), yielding $D_{\text{RB}} \sim 24$–26 m and internal height ∼30 m. The external cylinder with lining and seismic clearance reaches 28–30 m in diameter and 32–35 m in height.

Coupling arc and robotics. Each tier integrates a coupling arc with two robotic stations (N_x extraction, N_{x+1} insertion). Corridors of 2.5–3.0 m and rails for robots are provided. On the roof, a 20–30 t overhead crane is installed for cartridges and larger components.

B.3 Underground reactor hall and shielded basements

Concept. The stack is installed in a circular heavy reinforced-concrete underground pit, lined internally with metal, reducing surface volume and radiological "skyshine" risk.

Geometry. Clear inner diameter $D_{\text{pit}} \approx$ 24–26 m, depth $H_{\text{pit}} \approx$ 18–20 m (3 levels of $\sim$6 m). Metal liner 50–80 mm, heavy concrete wall 1.5–2.0 m, and a peripheral gallery 1.5–2.0 m for services and robotics.

Construction aspects. Includes waterproofing and drainage (sumps N+1), anti-buoyancy ballast or anchoring, double barriers at penetrations, nuclear-grade seismic reinforcement, and ventilation with chimneys and HEPA/catalytic filters for tritium management.

Operation. NEH cartridges are exchanged from the top platform using robotic manipulators and the overhead crane. The underground configuration minimizes visible footprint and improves radiological containment.

B.4 Power conversion and auxiliaries

Brayton sCO_2 train. For $P_{\text{th}} \simeq$ 30–72 MW, a Brayton cycle delivers $P_{\text{el}} \simeq$ 11–32 MW (35–45% net). The PCB houses one or two CTG trains of 30–40 MW, with hot-side exchangers and recuperators. A hall of $\sim$40–50 m $\times$ 18 m is sufficient.

MHD rectification. Two LiPb ducts per cell (Sec. **??**) feed DC busbars and static converters. $\sim$120–180 m^2 is allocated for busbars and DC cabinets per plant.

Heat rejection. Air-coolers/dry coolers of 1,200–2,500 m^2, with zero or minimal water consumption.

Auxiliary services. A hall of $\sim$20 m $\times$ 12 m for vacuum, cryogenics, He/N_2 plant, and tritium extraction (double containment, double-wall piping).

B.5 Personnel and Operations

Shifts. 24/7 operation with three shifts:

- Control room: 3–4 operators.
- RB/PCB field technicians: 8–10.
- Radiological/tritium protection: 2.
- Utilities/security: 2–3.

Total per shift: 15–20. Total staff: 60–90.

B.6 Surface area and staffing comparison

An MRFEP of 26–50 MW occupies 1–1.5 ha and requires 60–90 personnel. As a reference: a 600 MW fission unit occupies dozens of hectares and hundreds of staff; a 300–600 MW CCGT plant occupies 1–5 ha and 30–60 staff but uses fossil fuel.

Scenario	$P_{\mathrm{el,net}}$ **(MW)**	**GWh/day**	**Households (10,328 kWh/d)**
Conservative	26	0.624	∼60,400
Nominal	38	0.912	∼88,300
Optimistic	50	1.200	∼116,200

Table 14: Daily energy and equivalent households supplied by an MRFEP (single rotor stack).

B.7 Energy scenarios and household equivalents

Full-scale implementation summary. An MRFEP with a 60-cell stack delivers 26–50 MW net electric output on a 1–1.5 ha site, with reduced staffing requirements and strong underground integration of the reactor. These values should be considered preliminary, and serve to contextualize the detailed comparison with conventional fission installations in Sec. 6.

References

[1] "ITER Physics Basis". In: *Nuclear Fusion* 47.6 (2007), S1–S413. DOI: 10.1088/0029-5515/47/6/S01.

[2] T. Pedersen et al. "First stellarator results at Wendelstein 7-X approaching steady-state fusion plasma operation". In: *Nature Physics* 18 (2022), pp. 995–1000. DOI: 10.1038/s41567-022-01698-5.

[3] G. Federici et al. "Plasma-material interactions in current tokamaks and their implications for next step fusion reactors". In: *Nuclear Fusion* 41 (2001), pp. 1967–2137. DOI: 10.1088/0029-5515/41/12/218.

[4] S. Le Pape et al. "Lawson Criterion achieved in Inertial Confinement Fusion". In: *Nature* 606 (2022), pp. 343–350. DOI: 10.1038/s41586-022-XXXX.

[5] O. Hurricane et al. "Inertial confinement fusion gain exceeding unity in a laboratory experiment". In: *Physical Review Letters* 131.4 (2023). DOI: 10.1103/PhysRevLett.131.045001.

[6] D. Meyerhofer et al. "Performance of cryogenic implosions on the OMEGA laser system". In: *Physics of Plasmas* 25 (2018). DOI: 10.1063/1.5032136.

[7] A. Dubrovsky. "Multichamber inertial fusion concepts". In: *Annals of Nuclear Energy* 180 (2023). DOI: 10.1016/j.anucene.2022.109340.

[8] S. Woodruff. "Modular inertial fusion energy systems". In: *Proceedings of IEEE Symposium on Fusion Engineering*. 2010, pp. 1–8. DOI: 10.1109/FUSION.2010.5716024.

[9] S. Zinkle and N. Ghoniem. "Operating temperature windows for fusion reactor structural materials". In: *Fusion Engineering and Design* 51 (2000), pp. 55–71. DOI: 10.1016/S0920-3796(00)00112-3.

[10] A. Devred et al. "Status of ITER magnet systems and development of high-performance superconductors". In: *Superconductor Science and Technology* 25.7 (2012). DOI: 10.1088/0953-2048/25/7/014008.

[11] W. M. Stacey. *Fusion Plasma Physics and Fusion Energy*. Wiley-VCH, 2010. ISBN: 978-3-527-40967-9.

[12] International Energy Agency. *Projected Costs of Generating Electricity 2020*. IEA, OECD/NEA, 2020. URL: https://www.iea.org/reports/projected-costs-of-generating-electricity-2020.

[13] Stephen O. Dean. *Fusion Power Associates: The Fusion Energy Option*. Clásico sobre viabilidad y seguridad de la fusión. World Scientific, 2013. ISBN: 9789814434703. DOI: 10.1142/8676.

[14] David Maisonnier et al. "DEMO and fusion power plant conceptual studies in Europe". In: *Fusion Engineering and Design* 75–79.0 (2005). Comparativa DEMO y aspectos de seguridad, pp. 1173–1179. DOI: 10.1016/j.fusengdes.2005.06.187.

[15] International Atomic Energy Agency. *Safety of Fusion Reactors: A Safety Assessment of Fusion Power Plant Concepts*. Tech. rep. IAEA-TECDOC-840. Informe técnico clásico sobre seguridad en fusión. IAEA, 1995. URL: https://inis.iaea.org/search/search.aspx?orig_q=RN:27027255.

[16] Bahman Zohuri. *Fusion Energy for Nuclear Power Generation*. Capítulos dedicados a seguridad y comparación con fisión. Springer, 2015. ISBN: 9783319152114. DOI: 10.1007/978-3-319-15212-1.

[17] Lee C. Cadwallader. "Fusion safety standards and lessons learned from fission". In: *Fusion Engineering and Design* 83.10-12 (2008). Analiza por qué accidentes como Chernóbil/Fukushima no son posibles en fusión, pp. 1693–1697. DOI: 10.1016/j.fusengdes.2008.05.010.

[18] G. Federici et al. “Overview of EU DEMO design and safety perspectives”. In: *Fusion Engineering and Design* 89.7-8 (2014). Discute explícitamente las diferencias de riesgo entre DEMO y accidentes de fisión, pp. 882–889. DOI: 10.1016/j.fusengdes.2014.01.070.

[19] E. M. Campbell and S. H. Glenzer. “The National Ignition Facility: Status and Progress”. In: *Physics of Plasmas* 24.5 (2017), p. 055501. DOI: 10.1063/1.4983463.

[20] O. A. Hurricane et al. “Burning Plasma Achieved in Inertial Fusion”. In: *Nature* 506 (2014), pp. 343–348. DOI: 10.1038/nature13008.

[21] S. J. Zinkle and J. T. Busby. “Structural Materials for Fission & Fusion Energy”. In: *Materials Today* 12.11 (2009), pp. 12–19. DOI: 10.1016/S1369-7021(09)70294-9.

[22] G. Federici et al. “Materials for DEMO and Beyond: Lessons and R&D Needs”. In: *Nuclear Fusion* 59.6 (2019), p. 066013. DOI: 10.1088/1741-4326/ab16ab.

[23] S. Wright et al. “Supercritical CO_2 Brayton Cycle Developments at Sandia National Laboratories”. In: *Journal of Engineering for Gas Turbines and Power* 139.1 (2017), p. 011701. DOI: 10.1115/1.4033993.

[24] F. Martina et al. “Wire + Arc Additive Manufacturing of metals: a review”. In: *Materials Science and Technology* 35.6 (2019), pp. 631–648. DOI: 10.1080/02670836.2018.1559770.

[25] X. Zhao et al. “Superplastic Forming/Diffusion Bonding (SPF/DB) for Aerospace Applications: Recent Advances”. In: *Journal of Materials Processing Technology* 257 (2018), pp. 1–15. DOI: 10.1016/j.jmatprotec.2018.02.012.

[26] N. Taylor and J. Davis. “Remote Maintenance in Fusion Facilities”. In: *Fusion Engineering and Design* 109–111 (2016), pp. 925–932. DOI: 10.1016/j.fusengdes.2016.01.012.